Phys. Status Solidi B **251**, No. 9, 1801–1823 (2014) / **DOI** 10.1002/pssb.201350261

Part of Special Issue on
Semiconductor Spintronics

physica status solidi b
www.pss-b.com
basic solid state physics

Feature Article

Interplay of Rashba/Dresselhaus spin splittings probed by photogalvanic spectroscopy – A review

Sergey D. Ganichev[*,1] **and Leonid E. Golub**[2]

[1] University of Regensburg, 93040 Regensburg, Germany
[2] Ioffe Physical-Technical Institute of the RAS, 194021 St. Petersburg, Russia

Received 9 October 2013, revised 15 February 2014, accepted 20 February 2014
Published online 22 March 2014

Keywords photogalvanics, Rashba/Dresselhaus spin splittings, semiconductors

* Corresponding author: e-mail sergey.ganichev@ur.de, Phone: +49 941 9432050, Fax: +49 941 9431657

The paper reviews the interplay of Rashba/Dresselhaus spin splittings in various two-dimensional systems made of zinc-blende III–V, wurtzite, and SiGe semiconductors. We discuss the symmetry aspects of the linear and cubic in electron wavevector spin splitting in heterostructures prepared on (001)-, (110)-, (111)-, (113)-, (112)-, and (013)- oriented substrates and address the requirements for suppression of spin relaxation and realization of the persistent spin helix state. In experimental part of the paper, we overview experimental results on the interplay of Rashba/Dresselhaus spin splittings probed by photogalvanic spectroscopy: The method based on the phenomenological equivalence of the linear-in-wavevector spin splitting and several photogalvanic phenomena.

1 Introduction Quantum phenomena in semiconductors are highly sensitive to subtle details of the carrier energy spectrum so that even a small spin splitting of energy bands may result in measurable effects. A textbook example of the band spin splitting is the Zeeman effect, which is caused by the coupling of an external magnetic field and electron spin. However, band spin degeneracy can also be removed without action of a magnetic field. This phenomenon is caused by the spin–orbit interaction (SOI) in noncentrosymmetric crystals, a relativistic effect allowing for coupling of electron spin and orbital degrees of freedom. As a result the spin degeneracy of the energy bands is lifted even in nonmagnetic materials. This coupling is described by a Hamiltonian with products of $\boldsymbol{\sigma}$ and $\boldsymbol{k}$ terms where $\boldsymbol{\sigma}$ are the Pauli spin matrices and $\boldsymbol{k}$ is the electron wave vector. The origin of these terms are the bulk inversion asymmetry (BIA) and the structure inversion asymmetry (SIA). Microscopically, BIA stems from the absence of the inversion symmetry in the bulk material and gives rise to the Dresselhaus spin splitting in bulk and low-dimensional semiconductors [1, 2]. By contrast, SIA originates from the inversion asymmetry of the confining potential and yields the Rashba term in the Hamiltonian whose strength can be manipulated by an external electric field (Rashba effect) [3, 4]. In particular, the SIA/BIA coupling of the electron wavevector and spin causes a Larmor precession in an internal $\boldsymbol{k}$-dependent effective magnetic field for electrons moving through a semiconductor structure. Note that in addition to BIA and SIA, an interface inversion asymmetry (IIA) may yield $\boldsymbol{k}$-linear terms caused by noninversion symmetric bonding of atoms at heterostructure interfaces [5–7]. Since the IIA results in the SOI of the same form as BIA in (001)-grown III–V systems, we disregard this type of spin splitting in further consideration.

While the existence of the zero-magnetic field spin splitting is known since the 1960s of the last century [1, 3], it quickens an enormous interest since manipulation of the electron spin instead of its charge has been considered as a candidate for the future electronics – spintronics. The cause of this interest is that the Rashba effect in two-dimensional electron systems (2DES) provides a unique possibility to manipulate electron spin by means of external electric field and is of great importance for the generation, manipulation, and detection of spin currents as well as for control of the spin relaxation processes in low-dimensional semiconductors, for

reviews see Refs. [8–19]. In particular, spin manipulation by means of electric field, pure spin currents, and electric currents caused by spin polarization have attracted continuously growing interest from both the experimental and theoretical points of view. Most of these works are aimed to two-dimensional systems, where BIA and SIA terms couple the *in-plane* wavevector of confined electrons $\boldsymbol{k}$ with the *in-* or *out-of-plane* components of the electron spin $\boldsymbol{S}$. The relative orientation of the coupled $\boldsymbol{k}$- and $\boldsymbol{S}$-components is determined by the symmetry of the system. Consequently, it depends on the QW growth plane crystallographic orientation and on the considered direction of the in-plane wavevector. In many systems, the SIA and BIA terms can interfere resulting in an anisotropy of the spin splitting. The strongest anisotropy can be achieved in (001)-grown quantum wells (QWs) with the $\boldsymbol{k}$-linear Rashba and Dresselhaus terms of equal strength. Under these circumstances, the dominant mechanism of spin dephasing (Dyakonov–Perel relaxation [20]) is suppressed [21–23] making possible a diffusive spin field transistor [24] as well as giving rise to a persistent spin helix (PSH) predicted in Ref. [25] and observed in GaAs low-dimensional systems [26, 27]. In fact, for this particular case, the spin splitting vanishes in certain $\boldsymbol{k}$-space directions and an effective magnetic field caused by SOI is aligned along a certain crystallographic axis for all $\boldsymbol{k}$ being ineffective for spins oriented along this axis, see, e.g., Refs. [22, 24, 28]. Further important example of the SIA/BIA anisotropy is manipulation of the spin dephasing in QWs grown on (110) or (111) crystallographic planes where extremely long spin relaxation times have been experimentally achieved by adjusting of Rashba and Dresselhaus spin splitting [29–42]. Lately, there has been much effort in the studying of the SIA/BIA-interplay both theoretically with new device proposals [24, 43–46] and experimentally with the aim to obtain particular relation between SIA and BIA spin splitting in QW systems of various crystallographic orientations.

Owing to the fact that Rashba/Dresselhaus zero magnetic field spin splittings give rise to a large number of diverse physical phenomena their characterization and control are of fundamental importance for spin physics in semiconductors. The relative orientation of spin and electron wavevector in eigenstates and strength of these splittings depend on macroscopic conditions such as structure crystallographic orientation, QW width, temperature, electron density, doping profile, stress, etc. Consequently, the interplay of the Rashba/Dresselhaus spin splittings is strongly affected by these parameters and requires a detailed study. Various methods providing an experimental access to the SIA/BIA interplay have been developed to which belong (i) investigations of the anisotropy of the Raman effect [47, 48]; (ii) study of the weak antilocalization (WAL) [49–53] and WAL in tilted magnetic fields [54–57]; (iii) photogalvanic effects [33, 58–66]; (iv) investigation of spin-relaxation anisotropy by Hanle-effect [67]; (v) study of the gate dependence of spin relaxation [68–71], as well as (vi) experiments on time resolved Kerr effect (TRKR) or Faraday rotation in special experimental geometries [72–79], including magnetooptical Kerr effect with in-plane magnetic fields [74] and optical monitoring the angular dependence of the electron spin precession on their direction of motion with respect to the crystal lattice [75]. The multifaceted SIA/BIA spin splitting has been the subject of a tremendous number of works and numerous reviews. Our contribution to this special issue is primary focused on the results obtained in the framework within the DFG Schwerpunktprogramm SPP 1285 and, consequently, limited to the investigation of SIA/BIA explored by study of the photogalvanic effects anisotropy. The developed methods are based on the phenomenological equivalence of SIA/BIA spin splitting and several photogalvanic phenomena [28, 80, 81], which all have a common property: They are described by the linear coupling of a polar vector and an axial vector, like the electron wavevector with its spin in Rashba/Dresselhaus effect or, e.g., electric current with an average nonequilibrium spin in the spin-galvanic effect [58]. Indeed, such phenomena are described by second rank pseudo-tensors whose irreducible components differ by a scalar factor only. Therefore, these methods allow determination of the spin–orbit coupling anisotropy in 2DES and do not require a knowledge of microscopic details or rely on theoretical quantities. Furthermore, previous studies demonstrated that the discussed effects are very general and measurable signals can be obtained for almost all 2DES and even at room temperature, for reviews see, e.g., Ref. [80]. Thus, photogalvanic experiments allow us characterization of the SIA/BIA interplay upon variation of macroscopic parameters in a wide range.

The paper is organized in the following way: In Section 2, an overview of the symmetry aspects of the Rashba/Dresselhaus effects in III–V semiconductor materials is given. First the removal of spin degeneracy due to spin–orbit interaction is addressed and then the SIA/BIA spin splitting in $\boldsymbol{k}$-space for 2DES grown in various crystallographic directions is presented. Sections 3 and 4 introduce the method based on photogalvanics and give a short account for the experimental technique, respectively. The experimental results on interplay of SIA/BIA upon variation of 2DES design and characteristics are presented and discussed in Sections 5 (zinc-blende III-V-based QWs), 6.1 (wurtzite 2DES), and 6.2 (SiGe QWs). Conclusions and outlook are given in Section 7.

2 Symmetry analysis of the Rashba/Dresselhaus band spin splitting in zinc-blende materials

In the absence of external magnetic fields, the time inversion results in the Kramers theorem which reads as $\varepsilon_{\uparrow}(\boldsymbol{k}) = \varepsilon_{\downarrow}(-\boldsymbol{k})$. Here, ε is electron energy, and $\uparrow/\downarrow$ enumerate two spin states. If the system has an inversion center then, applying the space inversion operation, one gets $\varepsilon_{\uparrow}(\boldsymbol{k}) = \varepsilon_{\uparrow}(-\boldsymbol{k})$. Combining these two results, we see that two spin states with the same wavevector $\boldsymbol{k}$ have the same energy and the electron energy spectrum close to the conduction band minima is well described by a parabolic dispersion: $\varepsilon_{\uparrow}(\boldsymbol{k}) = \varepsilon_{\downarrow}(\boldsymbol{k}) = \hbar^2 k^2/(2m^*)$, where m^* is the effective mass in the conduction band.

Table 1 Correspondence between growth-orientation dependent x, y, z labels and crystallografic orientations. Note that in (001)-grown III–V material-based QWs in a valuable number of works aimed to SIA/BIA spin splitting cubic axes with $x' \parallel [100]$ and $y' \parallel [010]$ are used.

	growth plane					
	zinc-blende and SiGe					wurtzite
	bulk	(001)	(110)	(111)	(113)	
x	[100]	$[1\bar{1}0]$	$[\bar{1}10]$	$[11\bar{2}]$	$[1\bar{1}0]$	$[11\bar{2}0]$
y	[010]	[110]	[001]	$[\bar{1}10]$	$[33\bar{2}]$	$[1\bar{1}00]$
z	[001]	[001]	[110]	[111]	[113]	[0001]

However, in the system lacking an inversion center, e.g., zinc-blende and wurtzite bulk semiconductors and 2DES, the spin splitting can be present even in zero magnetic field. Such a splitting is caused by SOI. The corresponding Hamiltonian H_{SO} is given by a sum of products of the Pauli matrices and odd combinations of the wavevector components. In bulk III–V semiconductors belonging to T_d point group symmetry it is described by the cubic in the wavevector $\boldsymbol{k}$ terms introduced by Dresselhaus [1]:

$$H_{\text{bulk}} = \gamma[\sigma_x k_x(k_y^2 - k_z^2) + \sigma_y k_y(k_z^2 - k_x^2) + \sigma_z k_z(k_x^2 - k_y^2)]. \quad (1)$$

Here, γ is the only one linearly-independent constant for the T_d point group and x, y, z are cubic axes. Note that hereafter the crystallographic orientation of x, y, z axes for each considered system is given in Table 1. Despite this splitting determines the Dyakonov–Perel spin relaxation rate, its value can not be manipulated by an electric field and is determined by the constant γ.

In 2D systems, confinement and symmetry lowering result in a more rich SOI, which is described by new terms in the Hamiltonian both, linear and cubic, in the electron 2D wavevector. The corresponding spin–orbit splitting is sensitive to external parameters like electric field, temperature, structure design, crystallographic orientation, etc. Below we consider one by one QW structures grown in various directions. The three point groups D_{2d}, C_{2v}, and C_s are particularly relevant for zinc-blende structure-based QWs [28, 82, 83]. Hereafter, the Schönflies notation is used to label the point groups. In the international notation, they are labeled as $\bar{4}2m$, $mm2$, and m, respectively.

2.1 Rashba/Dresselhaus terms in (001)-grown zinc-blende structure-based 2DES Quantum well structures made of III–V semiconductors MBE grown on (001)-oriented substrates are the most studied low-dimensional systems. The point symmetry group of these structures can be either D_{2d} or C_{2v} which both belong the gyrotropic point groups [84] and, consequently allow linear in wavevector spin splitting. The D_{2d} symmetry corresponds to (001)-oriented symmetrical QWs. In such QWs, only BIA terms may exist. If an additional up-down asymmetry is present due to, e.g., nonequivalent interfaces, asymmetric doping, or electric field applied normally to QW plane, then the symmetry is reduced to C_{2v} giving rise to SIA. For these QWs the tensor elements can be conveniently presented in the coordinate system (xyz) with $x \parallel [1\bar{1}0]$, $y \parallel [110]$, $z \parallel [001]$, see Table 1 and Fig. 1a. The axes x and y lie in the reflection planes m_1 and m_2 of both point groups and are perpendicular to the principal twofold rotation axis C_2, see Fig. 1b showing symmetry elements for QWs of C_{2v} point group.

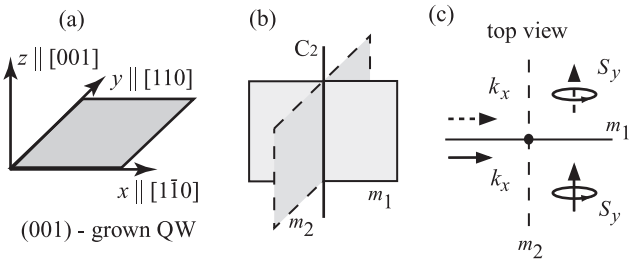

Figure 1 (a) Coordinate system used for (001)-grown III–V QWs, (b) symmetry elements of the C_{2v} point group: mirror planes m_1 and m_2 and C_2-axis in the QW grown along $z \parallel [001]$. Arrows in the drawing (c) show that the reflection in the mirror plane m_1 does not change the sign of both the polar vector component k_x and the axial vector component S_y, demonstrating that a linear coupling between k_x and S_y is allowed under this symmetry operation. This coupling is also allowed by the other symmetry operations (mirror reflection by the plane m_2 at which both components change their sign and the C_2 rotation axis) of the point group yielding the $k_x\sigma_y$ terms in the effective Hamiltonian.

For D_{2d} point symmetry, the linear in $\boldsymbol{k}$ wavevector spin splitting is given by

$$H_{\text{BIA}} = \beta(\sigma_x k_y + \sigma_y k_x), \quad (2)$$

where β is called the (2D) Dresselhaus constant. It follows from Eq. (1) that the substantial contribution to β comes from the bulk spin–orbit coupling, which, taking into account that for confined electrons $\langle k_z \rangle$ becomes zero but $\langle k_z^2 \rangle$ does not, yields $\beta = -\gamma\langle k_z^2 \rangle$. Here, the brackets mean averaging over the size-quantized motion [2]. It is important to note, that historically many authors use coordinate axes directed along cubic axes, i.e., $x' \parallel [100]$ and $y' \parallel [010]$. As in this coordinate system x' and y' are tilted by 45° to the mirror planes, the other spin and $\boldsymbol{k}$ components are mixed and the form of the Hamiltonian changes. In this case, we have widely used in the literature form of $H_{\text{BIA}} = \beta(\sigma_{x'} k_{x'} - \sigma_{y'} k_{y'})$.

In the asymmetric QWs, belonging to C_{2v} point group and having nonequivalent z and $-z$ directions, SIA gives rise to additional terms in H_{SO} so that now $H_{SO} = H_{\text{BIA}} + H_{\text{SIA}}$. The form of H_{BIA} remains unchanged, see Eq. (2), and the SIA term assumes the form

$$H_{\text{SIA}} = \alpha(\sigma_x k_y - \sigma_y k_x) = \alpha(\boldsymbol{\sigma} \times \boldsymbol{k})_z, \quad (3)$$

where α is called the Rashba constant. Obviously the form of this term is independent of the orientation of Cartesian coordinates in the plane of the QW. Equations (2) and (3) show that linear in wavevector band spin splitting is possible for in-plane spin components only. This fact can be illustrated

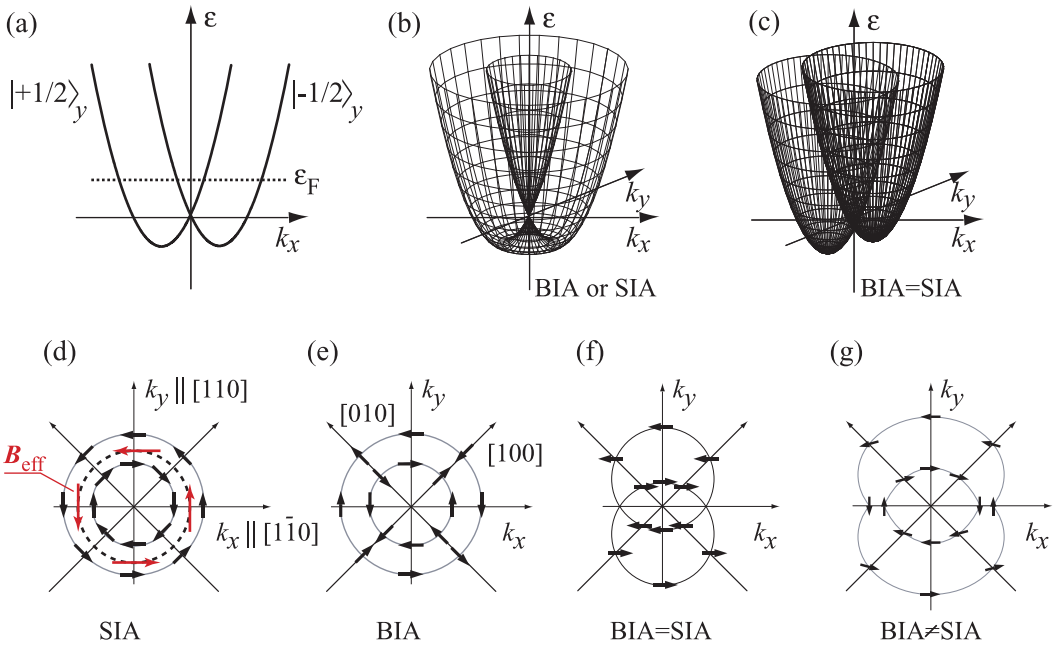

Figure 2 Panel (a) illustrates the SIA/BIA spin splitting due to $k_x\sigma_y$ terms in the effective Hamiltonian, here $|\pm 1/2\rangle_y$ label the eigenstates with fixed y spin components. Panels (b) and (c) show schematic 2D band structure with $\boldsymbol{k}$-linear terms for C_{2v} symmetry. The energy ε is plotted as a function of k_x and k_y in (b) with only one type of inversion asymmetry, BIA or SIA, and in (c) for equal strength of the BIA and SIA terms in the Hamiltonian. The bottom panels (d–g) show the distribution of spin orientations at the Fermi energy for different strengths of the BIA and SIA terms. After [28, 58].

by simple symmetry arguments. It follows from the Neumann's principle that the component of a tensor representing a property must remain invariant under a transformation of coordinates governed by a symmetry operation valid for the point group of the crystal [92]. Therefore, the linear in $\boldsymbol{k}$ spin splitting can only occur for those components of $\boldsymbol{k}$ for which there are components of the pseudovector $\boldsymbol{S}$ (the corresponding quantum-mechanical operator is $\boldsymbol{\sigma}/2$) transforming in the same way. Let us illustrate it for spin aligned along y-direction, i.e., for S_y. Figure 1c shows the symmetry elements of asymmetric QWs (point group C_{2v}) together with the transformation of k_x and S_y by the mirror reflection in m_1 plane. We see, that the reflection in the plane m_1, as well as in m_2, transforms the wavevector component k_x and the pseudovector component S_y in the same way: $k_x \to k_x$, $S_y \to S_y$ for the plane m_1, see Fig. 1c, and $k_x \to -k_x$, $S_y \to -S_y$ for the plane m_2. As the remaining C_2-axis also transforms k_x and S_y equally the linear in $\boldsymbol{k}$ spin splitting connecting these components becomes possible yielding the $\sigma_y k_x$ terms in the effective Hamiltonians (2) and (3). The corresponding band structure is sketched in Fig. 2a. Similar arguments hold for k_y and S_x ($k_y\sigma_x$ terms), but not for the out-of-plane component S_z. Consequently, the linear in $\boldsymbol{k}$ spin splitting for out-of-plane spin is forbidden by symmetry.

The distribution of spin orientation in the states with a given $\boldsymbol{k}$ can be visualized by writing the SOI term in the form

$$H_{\rm SO} = \boldsymbol{\sigma} \cdot \boldsymbol{B}_{\rm eff}(\boldsymbol{k}), \tag{4}$$

where $\boldsymbol{B}_{\rm eff}(\boldsymbol{k})$ is an effective magnetic field (with absorbed Bohr magneton and g^*-factor [93]), which provides the relevant quantization axes. The index "effective" indicates that $\boldsymbol{B}_{\rm eff}(\boldsymbol{k})$ is not a real magnetic field because it does not break the time-inversion [94]. Consequently, in the presence of SIA/BIA spin splitting the Kramers-relation $\varepsilon_\uparrow(\boldsymbol{k}) = \varepsilon_\downarrow(-\boldsymbol{k})$ holds. By comparison of Eq. (4) with Eqs. (2) and (3) one obtains for pure SIA ($\beta = 0$) and pure BIA ($\alpha = 0$) the effective magnetic fields in forms

$$\boldsymbol{B}_{\rm eff}^{\rm SIA} = \alpha(k_y, -k_x), \qquad \boldsymbol{B}_{\rm eff}^{\rm BIA} = \beta(k_y, k_x). \tag{5}$$

The effective magnetic field and spin orientations for, both, Rashba and Dresselhaus coupling are schematically shown by arrows in Fig. 2d and e, respectively. Here, it is assumed for concreteness that $\alpha, \beta > 0$. For the SIA case, the effective magnetic field and, hence, the electron spin in the eigenstates with the wavevector $\boldsymbol{k}$ are always perpendicular to the $\boldsymbol{k}$-vector, see Fig. 2d. By contrast, for the BIA contribution, the angle between $\boldsymbol{k}$-vector and spins depends on the direction of $\boldsymbol{k}$, see Fig. 2e. In the presence of both SIA and BIA spin–orbit couplings (C_{2v} symmetry), the $[1\bar{1}0]$ and the $[110]$ axes become strongly nonequivalent. For $\boldsymbol{k} \parallel [1\bar{1}0]$, the eigenvalues of the Hamiltonian are then given by $\varepsilon_\pm = \hbar^2k^2/2m^* \pm (\alpha - \beta)k$ and for $\boldsymbol{k} \parallel [110]$ by $\varepsilon_\pm = \hbar^2k^2/2m^* \pm (\alpha + \beta)k$. For an arbitrary direction of $\boldsymbol{k}$, the energy spectrum of such systems consists of two branches

with the following anisotropic dispersions

$$\varepsilon_{\pm}(\boldsymbol{k}) = \frac{\hbar^2 k^2}{2m^*} \pm k\sqrt{\alpha^2 + \beta^2 + 2\alpha\beta \sin 2\vartheta_{\boldsymbol{k}}}\ , \tag{6}$$

where $\vartheta_{\boldsymbol{k}}$ is the angle between $\boldsymbol{k}$ and the x axis [98, 99]. The energy dispersion for $\boldsymbol{k}$-linear SIA, BIA and combined SIA/BIA terms is illustrated in Fig. 2a–c. In the case of BIA only ($\alpha = 0$) or SIA only ($\beta = 0$), the band structure is the result of the revolution around the energy axis of two parabolas symmetrically displaced with respect to $\boldsymbol{k} = 0$. The interplay of SIA and BIA is illustrated in panels (d–g). If the strengths of BIA and SIA are the same, then the 2D band structure consists of two revolution paraboloids with revolution axes symmetrically shifted in opposite directions with respect to $\boldsymbol{k} = 0$, see Fig. 2c. Now all spins are oriented along $\pm x$-axes as shown in Fig. 2f. In Fig. 2g, we have shown a constant energy surface and direction of spins for $\alpha \neq \beta$.

So far we discussed only $\boldsymbol{k}$-linear terms in the Hamiltonian. In fact, in zinc-blende structure based (001)-grown QWs also terms cubic in $\boldsymbol{k}$ are present, which stem from the Dresselhaus term in the host bulk material, Eq. (1). A cubic contribution modifies the Dresselhaus spin-splitting yielding

$$H_{\mathrm{BIA}}^{\mathrm{cub}} = \frac{\gamma}{2}\left(\sigma_x k_y - \sigma_y k_x\right)\left(k_y^2 - k_x^2\right). \tag{7}$$

These terms influence some of spin-dependent phenomena like spin relaxation or WAL and should be taken into account in particularly in narrow band materials and highly doped QWs as well as at high temperature. The corresponding $\boldsymbol{k}$-cubic effective magnetic field defined via $H_{\mathrm{BIA}}^{\mathrm{cub}} = \boldsymbol{\sigma} \cdot \boldsymbol{B}_{\mathrm{cub}}$ can be conveniently decomposed into $\boldsymbol{B}_{\mathrm{cub}} = \boldsymbol{B}_{\mathrm{cub}}^{(1)} + \boldsymbol{B}_{\mathrm{cub}}^{(3)}$, where [96]

$$\begin{aligned} \boldsymbol{B}_{\mathrm{cub}}^{(1)} &= -\frac{\gamma k^2}{4}(k_y, k_x), \\ \boldsymbol{B}_{\mathrm{cub}}^{(3)} &= \frac{\gamma k^3}{4}\left(\sin 3\vartheta_{\boldsymbol{k}}, -\cos 3\vartheta_{\boldsymbol{k}}\right)\ . \end{aligned} \tag{8}$$

As the effective magnetic fields $\boldsymbol{B}_{\mathrm{eff}}^{\mathrm{BIA}}$ and $\boldsymbol{B}_{\mathrm{cub}}^{(1)}$ containing the first-order Fourier harmonics ($\propto \sin\vartheta_{\boldsymbol{k}}$ and $\cos\vartheta_{\boldsymbol{k}}$) have the same form [see Eqs. (5) and (8)] they can be combined as

$$\boldsymbol{B}_{\mathrm{eff}}^{(1)} = \boldsymbol{B}_{\mathrm{eff}}^{\mathrm{BIA}} + \boldsymbol{B}_{\mathrm{cub}}^{(1)} = \tilde{\beta}(k_y, k_x) \tag{9}$$

with the renormalized Dresselhaus constant

$$\tilde{\beta} = \beta - \frac{\gamma k^2}{4}. \tag{10}$$

Note that the term $\gamma k^2/4$ scales with k, which for equilibrium electron gas is equal to the Fermi wavevector and respectively, scales with the electron density. In GaAs heterostructures, cubic in $\boldsymbol{k}$ terms are usually unimportant and in the further consideration we will use $\tilde{\beta}$ for analysis of narrow band semiconductors only.

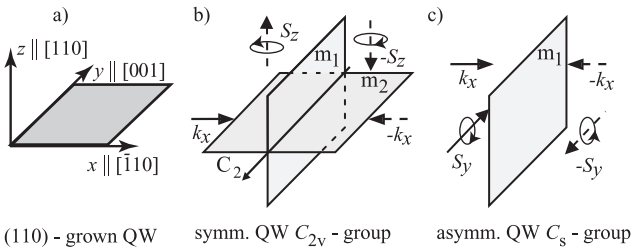

Figure 3 (a) Coordinate system of the (110)-grown III–V QW. (b) Mirror planes m_1 and m_2 and C_2-axis in symmetric QW belonging to C_{2v} point group. (c) Remaining symmetry elements in asymmetric QWs (C_s point group). Arrows in the drawing (b) show that the reflection in the mirror plane m_1 changes the sign of both the polar vector component k_x and the axial vector component S_z, demonstrating that a linear coupling of k_x and S_z is allowed under this symmetry operation. This coupling is also allowed by the other symmetry operations (mirror reflection by the plane m_2 and the C_2 rotation axis) of the point group yielding the $\sigma_z k_x$ terms in the effective Hamiltonian. By contrast, the in-plane spin $\boldsymbol{S}$ at reflection in plane m_2 transforms differently compared to any in-plane wavevector components. Arrows in the sketch (c) demonstrate that in asymmetric QWs for which m_2 is removed, the coupling between the in-plane spin S_y and wavevector component k_x becomes possible. Same arguments are valid for the coupling of S_x and k_y. Thus, SIA in asymmetric QWs results in the in-plane effective magnetic field and gives rise to the Dyakonov–Perel spin relaxation for spins oriented along the growth direction.

2.2 Rashba/Dresselhaus terms in (110)-grown zinc-blende structure-based 2DES QWs on (110)-oriented GaAs substrates attracted growing attention due to their extraordinary slow spin dephasing, which can reach several hundreds of nanoseconds [29–33, 35, 36, 38]. As addressed above, the reason for the long spin lifetime in this type of QWs is their symmetry: in (110)-grown QWs, the BIA effective magnetic field $\boldsymbol{B}_{\mathrm{eff}}(\boldsymbol{k})$ points into the growth direction [2] therefore spins oriented along this direction do not precess. Hence the Dyakonov–Perel spin relaxation mechanism, which is based on the spin precession in $\boldsymbol{B}_{\mathrm{eff}}(\boldsymbol{k})$ and usually limits the spin lifetime of conduction electrons, is suppressed.

Depending on the equivalence or nonequivalence of the QW interfaces, i.e., presence or absence of SIA, the structure symmetry may belong to one of the point groups: C_{2v} or C_s, respectively. While the point group symmetry of symmetric (110)- and asymmetric (001)-oriented III–V QWs is the same (C_{2v}), the Dresselhaus spin splitting links different components of electron spin and wavevector. The reason for this fact, strange on the first glance, is that by contrast to (001)-oriented QWs for which mirror reflection planes m_1 and m_2 are oriented normal to the QW plane, see Fig. 1, in symmetric (110) QWs one of the planes, say m_2, coincides with the plane of QW. The symmetry elements of symmetrical (110)-grown QWs are shown in Fig. 3b. By simple symmetry analysis we find that the only wavevector and spin components transforming in the same way are k_x and S_z, i.e., the effective magnetic field caused by the spin splitting points along the

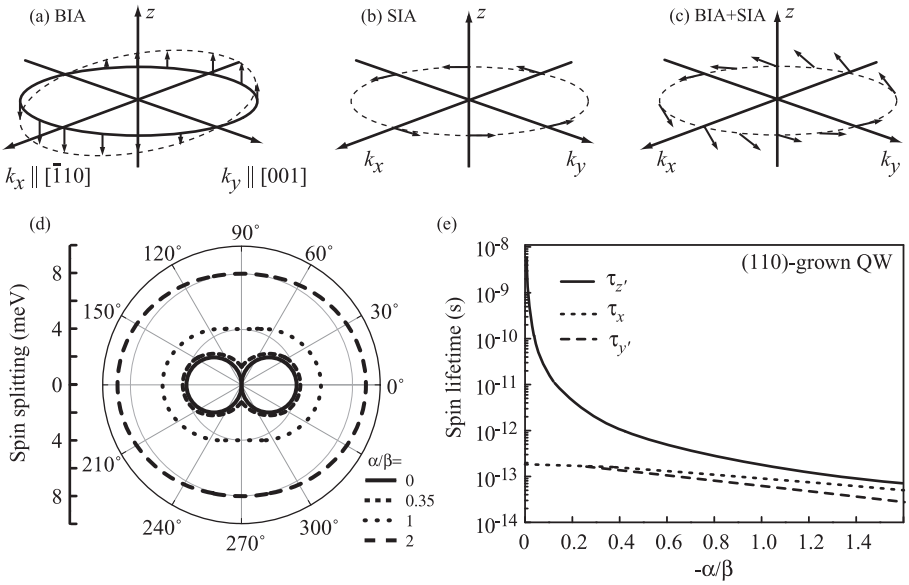

Figure 4 (a–c) Crystallographic directions and effective magnetic fields for the lower conduction subband in (110)-grown QW. Plots (a–c) sketch $B_{\rm eff}(\boldsymbol{k})$ for BIA, SIA, and SIA/BIA interplay, respectively. Note that for α=0, panel (a), $B_{\rm eff}(\boldsymbol{k})$ is aligned along z axis for any $\boldsymbol{k}$ apart from $\boldsymbol{k} \parallel y$ at which states are spin degenerated. (d) Calculated values of the spin splitting for states lying on a circle in the k_x–k_y plane with $k = 0.01$ Å^{-1} for various α/β ratio. Here, β is 10^{-9} eV cm is assumed for calculations. (e) Spin lifetimes as a function of the ratio of the SIA and the BIA parameters. The labels $\tau_{x,y',z'}$ refer to the spin relaxation tensor in the axes x, y', and z'. The latter two lie in (y, z) plane and are tilted to the axes y and z, see Table 1, by the angle $\theta = \arctan(\alpha/\beta)$. Data are given after [103].

growth axis. The reflection of these components in the m_1 mirror plane resulting in $k_x \to -k_x$, $S_z \to -S_z$, are shown in Fig. 3b. The corresponding Hamiltonian has the form

$$H_{\rm BIA} = \beta \sigma_z k_x. \tag{11}$$

SIA removes the mirror reflection plane m_2 and enables spin splitting for the in-plane spin components. This is illustrated in Fig. 3c showing that in asymmetric (110)-grown structures k_x and S_y transform equally. Additional terms in the Hamiltonian caused by the symmetry reduction have the same form as the Rashba terms in (001)-oriented QWs Eq. (3). The in-plane effective magnetic field due to Rashba spin–orbit coupling results in spin dephasing even for spins oriented along growth direction and the benefit of (110) QWs disappears [100]. The energy spectrum of such systems consists of two branches with the following anisotropic dispersions

$$\varepsilon_{\pm}(\boldsymbol{k}) = \frac{\hbar^2 k^2}{2m^*} \pm k\sqrt{\alpha^2 + \beta^2 \cos^2 \vartheta_{\boldsymbol{k}}}\ . \tag{12}$$

Like in (001) QWs, the different forms of the BIA and SIA terms result in their interference substantially affecting the band spin-splitting. The spin splitting and calculated spin relaxation times for some α/β-ratios are shown in Fig. 4d and e, respectively. Moreover, the $\boldsymbol{k}$-cubic terms for symmetric (110) QWs result in the effective magnetic field also pointing in the growth direction, so they do not lead to spin relaxation of the normal spin component as well.

2.3 Rashba/Dresselhaus terms in (111)-grown zinc-blende structure-based 2DES QWs grown along [111]-direction draw attention primary due to the possible suppression of the Dyakonov–Perel spin relaxation mechanism for all spin components [37, 39–42, 103–105]. The reason for this interesting feature is the formal identity of the $\boldsymbol{k}$-linear Dresselhaus and Rashba Hamiltonians, which both have a form of Eq. (3) but imply different constants, β and α, respectively [2, 103]. As a result, the total spin–orbit Hamiltonian can be written in form

$$H_{\rm SO} = (\beta + \alpha)(\sigma_x k_y - \sigma_y k_x). \tag{13}$$

The corresponding effective magnetic fields are shown in the inset in Fig. 5. A straightforward consequence of Eq. (13) is that conduction band becomes spin degenerate to first order in $\boldsymbol{k}$ for *any* wavevector direction in the case that BIA and SIA coefficients would have equal magnitude but opposite signs, i.e., $\beta = -\alpha$. The most significant feature of this configuration is that the spin lifetimes would become tremendously increased. The dependence of the in-plane and out-of-plane spin relaxation times on the ratio between the Rashba and Dresselhaus coefficients is shown in Fig. 5.

2.4 Rashba/Dresselhaus terms in (113)-, (112)-, (013)-, and *miscut* (001)-grown zinc-blende structure-based 2DES So far we discussed widely spread configurations of zinc-blende structure-based QWs. To be complete, we also address the band spin splitting in QWs grown in more exotic directions. These are (113)-,

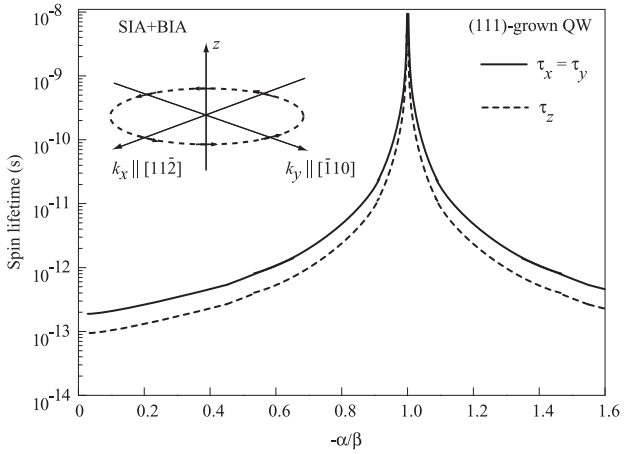

Figure 5 Spin lifetimes in (111)-grown QW as a function of the SIA/BIA-ratio. Inset sketches $\boldsymbol{B}_{\rm eff}(\boldsymbol{k})$ for QWs with any values of SIA/BIA ratio. Note that in the case of $\beta = -\alpha$ effective magnetic field $\boldsymbol{B}_{\rm eff}(\boldsymbol{k}) = 0$ for any electron wavevector and states become spin degenerated. Data are given after [103].

(112)-, and (013)-oriented 2DES as well as (001) *miscut* structures. The former orientation is usually used for growth of high mobility p-type GaAs QWs, which attracted notable attention due to the possibility to obtain long spin relaxation times [106–112]. QWs of (112)- and (013)-orientations are mainly used for growth of HgTe 2DES, which become particularly important since discovery of the topological insulator states in this material [113, 114] opening the possibility to study physics of Dirac fermions in the systems with the strong SOI. Miscut heterostructures are usually MOCVD-grown on slightly tilted (001) substrates.

Zinc-blende structure based (113)-, (112)- and *miscut* (001)-oriented 2DES belong to the symmetry point group C_s, which contains only two elements, the identity and one mirror reflection plane, m, being normal to the 2DES plane. A natural coordinate system for these structures grown in z-direction are x - normal to the plane m and y-orthogonal to x and z, cf. Table 1 for (113)-grown QWs. Then BIA spin-splitting is given by

$$H_{\rm BIA}^{\rm C_s} = \beta_1 \sigma_x k_y + \beta_2 \sigma_y k_x + \beta_3 \sigma_z k_x \ , \tag{14}$$

while the SIA Hamiltonian is again described by a universal form of Eq. (3). A particular feature of such 2DES compared to (001)-grown QWs is the appearance of the spin splitting for spins oriented along the growth direction. Note that the spin–orbit coupling terms in asymmetric (110) QWs, which have C_s symmetry, are also described by the sum of the Hamiltonians Eqs. (3) and (14).

QWs prepared on (013)-oriented substrates belong to the trivial point group C_1 lacking any symmetry operation except the identity. This is true even for structure-symmetric QWs, where SIA is absent. Hence, symmetry does not impose any restriction on the relation between the spin and wavevector components:

$$H_{\rm SO}^{\rm C_1} = \sum_{lm} \Lambda_{lm} \sigma_l k_m . \tag{15}$$

Here $l = x, y, z$ and $m = x, y$. Since all components of the pseudotensor $\boldsymbol{\Lambda}$ may be different from zero the spin splitting is allowed for any relative directions of spin and electron wavevector. Moreover, the ratio between the components of the tensor $\boldsymbol{\Lambda}$ can be changed in nontrivial way (including the sign inversion) by varying the experimental conditions like, e.g., sample temperature or carrier density.

To complete the picture of spin splitting in zinc-blende structure-based QWs, we note that symmetry reduction can also be obtained by, e.g., applying stress, fabricating ungated/gated lateral superlattices, and growing quasi one-dimensional wires. The form of the spin–orbit Hamiltonian in such structures depends on the resulting symmetry (C_{2v}, C_s, or C_1) and is described by the corresponding equations discussed above.

2.5 Wurtzite-type semiconductor structures Wurtzite-type bulk semiconductors, like GaN or InN, are described by a nonsymmorphic space group C_{6v}^4 containing a nontrivial translation. However, the physical effects are determined by the point-group symmetry. The point group of wurtzite semiconductors C_{6v} is gyrotropic [84] and, therefore, allows the linear in wavevector spin splitting. As it was pointed out in Ref. [3] in these media the spin–orbit part of the Hamiltonian has the form

$$H_{\rm bulk} = \beta(\boldsymbol{\sigma} \times \boldsymbol{k})_z , \tag{16}$$

where the constant β is solely due to BIA. Here, z-axis is directed along the hexagonal c-axis [115]. In heterostructures, an additional source of $\boldsymbol{k}$-linear spin splitting, induced by SIA becomes possible. If both, bulk and structure asymmetries, are present the resulting coupling constant is equal to the sum of BIA and SIA contributions to the spin–orbit part of the Hamiltonian. Thus, for 2DES based, e.g., on GaN or InN grown in [0001] direction, the total spin–orbit part of the Hamiltonian has exactly the same form as that for (111)-grown zinc-blende based structures discussed in Section 2.3:

$$H_{\rm SO} = (\beta + \alpha)(\sigma_x k_y - \sigma_y k_x) , \tag{17}$$

and for $\beta = -\alpha$ conduction bands become spin degenerate to first order in $\boldsymbol{k}$ for *any* wavevector direction.

2.6 SiGe QWs Finally, we briefly discuss SiGe QWs. Since both Si and Ge possess inversion center SiGe heterostructures do not have BIA. However, both IIA, with a BIA-like form of the Hamiltonian [117], and SIA may lead to $\boldsymbol{k}$-linear terms [116, 118–122]. The symmetry of $Si/(Si_{1-x}Ge_x)_n/Si$ QW in the absence of SIA depends on the number n of the mono-atomic layers in the well. In the case of

(001)-grown QW structures with an even number n, the symmetry of QWs is D_{2h} which is inversion symmetric and does not yield $\boldsymbol{k}$-linear terms. An odd number of n, however, interchanges the $[1\bar{1}0]$ and $[110]$ axes of the adjacent barriers and reduces the symmetry to D_{2d} [116, 119] with the same implication treated above for zinc-blende structure-based QWs, see Eq. (2) for IIA. The symmetry reduction of SiGe structures to C_{2v} may be caused by, e.g., an electric field (external or built-in) applied along the growth direction. If the structure is grown along the low-symmetry axis $z \parallel [hhl]$ with $[hhl] \neq [001]$ or $[111]$, the point group becomes C_s (see, e.g., [116]) and contains only two elements, the identity and one mirror reflection plane $(1\bar{1}0)$. Here, the spin splitting is described by equations presented in Section 2.4.

3 Determination of SIA and BIA spin splittings by photogalvanic measurements A direct way to explore the BIA and SIA interplay, which does not require knowledge of microscopic details, is based on the phenomenological equivalence of Rashba/Dresselhaus linear in $\boldsymbol{k}$ spin splitting given by

$$H_{\mathrm{SO}} = \sum_{lm} \Lambda_{lm} \sigma_l k_m, \tag{18}$$

where Λ_{lm} is a second rank pseudo-tensor, with other phenomena also described by a linear coupling of a polar vector, like current, and an axial vector, like electron spin. Indeed, all these effects are described by second rank pseudo-tensors whose irreducible components differ by a scalar factor only and, consequently, are characterized by the same anisotropy. In semiconductor 2DES, there are three effects, which belong to a large class of photogalvanic phenomena [80, 82, 83, 123, 124] and like Rashba/Dresselhaus linear in $\boldsymbol{k}$ spin splitting are described by such a kind of the second rank pseudo-tensors. These phenomena are the spin-galvanic effect (SGE) [125, 126], the circular photogalvanic effect (CPGE) [127, 128], and magneto-gyrotropic effect (MPGE) [60, 129]. They link the dc electric current with nonequilibrium spin (SGE), angular momentum of photons (CPGE) or an external magnetic field (MPGE). In analogy to the band spin-splitting and based on the equivalence of the invariant irreducible components of the corresponding pseudo-tensors, these currents can be decomposed into Rashba and Dresselhaus contributions, which can be measured separately. Taking the ratio between these contributions cancels the scalar factor, which contains all microscopic details [33, 58–60, 64, 130, 131]. As the physical mechanisms of the effects under consideration are discussed in a great details in several reviews and monographs [11, 28, 80, 83, 145] and are in fact inessential for the study of the the spin-splitting anisotropy we focus below on their symmetry analysis. We start with the general equations for each effect and briefly address their origin.

(i) Spin-galvanic effect. The spin-galvanic effect consists in the generation of an electric current $\boldsymbol{j}$ due to a nonequilibrium spin $\boldsymbol{S}$ and is caused by an asymmetric spin relaxation in the Rashba/Dresselhaus spin-split subbands [28, 80]. The spin-galvanic effect generally does not need an optical excitation but may also occur due to optical spin orientation yielding a spin photocurrent. The resulting electric current is given by

$$j_l = \sum_m Q_{lm} S_m \ . \tag{19}$$

(ii) Circular photogalvanic effect. The CPGE is another phenomenon, which links the current to the spin-splitting in heterostructures [28, 80]. It steams from the selective photoexcitation of carriers in $\boldsymbol{k}$-space due to optical selection rules for absorption of circularly polarized light and is given by

$$j_l = \sum_m \chi_{lm} \hat{e}_m P_{\mathrm{circ}} |\boldsymbol{E}|^2 \ , \tag{20}$$

where $\hat{\boldsymbol{e}}$ is the unit vector pointing in the direction of light propagation, and $\boldsymbol{E}$ is the complex amplitude of the electric field of the electromagnetic wave. The direction of the resulting electric current reverses at inversion of the radiation helicity P_{circ} being a fingerprint of CPGE.

(iii) Magneto-gyrotropic effect. MPGE is the electric current excitation by normally incident radiation in the presence of an external magnetic field $\boldsymbol{B}$ [143, 144]. It may be caused by the spin or orbital mechanisms. The spin-driven MPGEs are based on spin–orbit coupling in 2DES with SIA and BIA. The electric current is generated due to a spin-dependent energy relaxation of electrons heated by radiation in the Zeeman split subbands. The orbital mechanism is caused by a magnetic-field-induced scattering asymmetry [195]. For unpolarized radiation MPGE is given by

$$j_l = \sum_m \xi_{lm} B_m |\boldsymbol{E}|^2 \ . \tag{21}$$

Equation (18) and (19)–(21) have in common that all these phenomena link linearly vector and pseudovector components. Therefore, as addressed above, they are characterized by the same anisotropy in space, according to the Neumann principle [92], the equivalence of the components of the pseudo-tensors $\boldsymbol{\Lambda}$, $\boldsymbol{Q}$, $\boldsymbol{\chi}$, and $\boldsymbol{\xi}$ can be used to evaluate the ratio between SIA and BIA strength as well as to determine their relative sign [33, 58–60, 64, 130, 131]. Note that the same arguments are valid for the inversed SGE [132].

This can be illustrated on example of the spin-galvanic effect where an electric current is caused by asymmetric spin relaxation of nonequilibrium spin polarized carriers in the system with a spin–orbit splitting of the energy spectrum, for reviews see [28, 81, 83]. While in general the spin-galvanic effect does not need optical excitation the SIA/BIA interplay can most convenient be studied applying circularly polarized radiation for spin orientation of carriers resulting in $\boldsymbol{S}$.

The SGE current $\boldsymbol{j}^{\mathrm{SGE}}$ is linked to the average spin by a second rank pseudo-tensor $\boldsymbol{Q}$, see Eq. (19), and can be

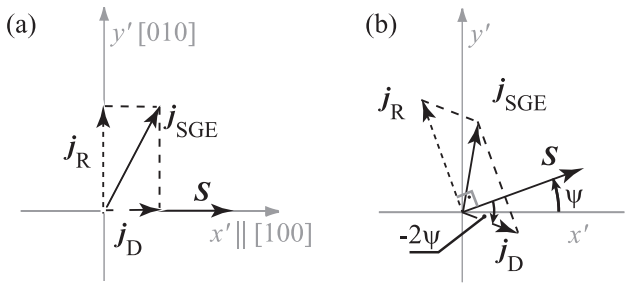

Figure 6 Spin-galvanic current and its SIA and BIA components in a (001)-grown QW: (a) for the in-plane average spin direction aligned along x', (b) for $\boldsymbol{S}$ given by arbitrary angle Ψ. After [58, 59].

presented via the parameters of spin–orbit splitting in (001) QWs as follows

$$j_x^{\mathrm{SGE}} = \tilde{Q}(\beta - \alpha)S_y, \qquad j_y^{\mathrm{SGE}} = \tilde{Q}(\beta + \alpha)S_x, \tag{22}$$

where $Q_{xy} = \tilde{Q}(\beta - \alpha)$, $Q_{yx} = \tilde{Q}(\beta + \alpha)$ with $\tilde{Q}$ being a constant determined by the kinetics of the SGE, namely by the characteristics of momentum and spin relaxation processes. In the coordinate system with cubic axes ($x' \parallel [100]$, $y' \parallel [010]$) Eq. (19) can be conveniently presented in the form

$$\boldsymbol{j}^{\mathrm{SGE}} = \tilde{Q} \begin{pmatrix} \beta & -\alpha \\ \alpha & -\beta \end{pmatrix} \boldsymbol{S}\,, \tag{23}$$

demonstrating that for spin aligned along x' or y' measurements of the SGE current parallel and perpendicular to $\boldsymbol{S}$ directly yield the α/β-ratio. This is sketched in Fig. 6a showing the average spin $\boldsymbol{S} \parallel x'$ and the spin-galvanic current $\boldsymbol{j}^{\mathrm{SGE}}$, which is decomposed into $j_{x'} = j_{\mathrm{D}}$ and $j_{y'} = j_R$ proportional to the Dresselhaus constant β and the Rashba constant α, respectively. This configuration represents the most convenient experimental geometry in which the ratio of the currents measured along x'- and y'-axes yields

$$\frac{\alpha}{\beta} = \frac{j_{y'}(\boldsymbol{S} \parallel x')}{j_{x'}(\boldsymbol{S} \parallel x')}\,. \tag{24}$$

We emphasize that this geometry unambiguously shows whether the Rashba or Dresselhaus contribution is dominating. Furthermore, these measurements provide experimental determination of both the ratio and the relative sign of the Rashba and Dresselhaus constants.

Analogously to the spin splitting, symmetry arguments yield that for arbitrary orientation of the average spin $\boldsymbol{S}$ the current $\boldsymbol{j}_{\mathrm{R}}$ is always perpendicular to $\boldsymbol{S}$ while the current $\boldsymbol{j}_{\mathrm{D}}$ encloses an angle -2Ψ with $\boldsymbol{S}$, where Ψ is the angle between $\boldsymbol{S}$ and the x'-axis. The strength of the total current j^{SGE} is given by the expression

$$j^{\mathrm{SGE}} = \sqrt{j_{\mathrm{R}}^2 + j_{\mathrm{D}}^2 - 2 j_{\mathrm{R}} j_{\mathrm{D}} \sin 2\Psi}\,, \tag{25}$$

which has the same algebraic form as the spin–orbit term in the band structure, see Eq. (6). Taking the ratio between Rashba and Dresselhaus current contributions cancels the scalar factor $\tilde{Q}$, which contains all microscopic details [58, 59]. Hence, by mapping the magnitude of the photocurrent in the plane of the QW the α/β-ratio can be directly extracted from experiments. Similar consideration can be made for the circular photogalvanic and MPGEs. The details of the method can be found in Refs. [33, 58–60, 80, 131, 143, 144].

An important advantage of the discussed method is that it applies to the photogalvanic effects, which are very general and have been detected in a large variety of low-dimensional semiconductor structures of a very different designs, for recent reviews on these effects see [80, 83, 91, 144, 145], including topological insulators and other systems with Dirac fermions [146–156]. The studies of the last decade show that these effects in 2DES can be detected in a wide temperature range including technologically important room temperature and applying radiation in a wide frequency range, from microwaves up to visible light. It is important to note that all photogalvanic effects addressed above are caused by the terms $\boldsymbol{B}_{\mathrm{eff}}^{(1)}(\boldsymbol{k})$ and $\boldsymbol{B}_{\mathrm{eff}}^{\mathrm{SIA}}(\boldsymbol{k})$ in the effective magnetic field, which are first angular harmonics of $\vartheta_{\boldsymbol{k}}$, see section 2.1. The rest cubic terms in the effective magnetic field $\boldsymbol{B}_{\mathrm{eff}}^{(3)}(\boldsymbol{k}) \propto \sin 3\vartheta_{\boldsymbol{k}}, \cos 3\vartheta_{\boldsymbol{k}}$ do not result in the discussed photogalvanic currents, however, they modify the spin-splitting and may affect spin relaxation and the anisotropy of spin-flip Raman scattering [48, 51, 79, 82, 157–159]. Consequently, photogalvanics based methods provide the information on the SIA/BIA terms given by Rashba constant α and renormalized Dresselhaus constant $\tilde{\beta}$.

4 Experimental technique Photogalvanics have been used to probe SIA/BIA interplay in a large variety of low-dimensional structures of different design yielding information on the modification of the SIA/BIA-ratio upon changing of various macroscopic parameters like crystallographic orientation, doping position, quantum well widths, temperature, etc. Zinc-blende and wurtzite semiconductor-based heterostructures as well as SiGe QWs were studied. For optical excitation, a great variety of radiation sources have been used including pulsed and cw molecular THz lasers [81, 146, 160–163], free electron lasers [81, 169, 164–168], CO_2 lasers [116, 168, 170], Ti-sapphire and other solid state lasers [62, 65, 171], semiconductor lasers [172, 173], He–Cd laser [174], time-domain THz systems [61, 81, 175–177], conventional Gunn diodes [178] etc. While SIA/BIA interplay has been studied in a wide frequency range from microwaves to the near infrared, microwaves/terahertz radiation are particularly suitable for the methods addressed in the previous section. First of all, in the microwave/terahertz range photogalvanics may be observed and investigated much more easily than in the visible or near infrared ranges, where strong spurious photocurrents, caused by other mechanisms like the Dember effect [81], photovoltaic effects at contacts, etc., mask the relatively weak spin photogalvanic

currents. Secondly, in contrast to conventional methods of optical spin orientation using interband transitions, terahertz radiation excites only one type of charge carrier yielding monopolar spin orientation, giving the information about spin splitting in one subband. Furthermore, electrons excited by terahertz radiation remain close to the Fermi energy, which corresponds to the conditions of electric spin injection.

Obviously photocurrent measurements applying radiation with photon energies smaller than the band gap require free carriers. Therefore, photogalvanic methods are applied to study either doped low-dimensional systems or undoped structures additionally exposed to light resulting in the photogeneration of electron–hole pairs. In the latter case, photogalvanics is caused by the superposition of electron and hole contributions, which complicates the analysis of the spin splitting in a particular band. Experimental geometry depends on the type of phenomenon used for the SIA/BIA mapping (CPGE, SGE, or MPGE) and crystallographic orientation of the studied low-dimensional structure. CPGE- and SGE-based methods require circularly polarized radiation at oblique, or, for low symmetric structures, normal incidence. For MPGE- [60, 179] and, in some cases, SGE-based methods [58], a small external magnetic field is needed. Details of the experimental configurations can be found in Refs. [33, 58–60, 80, 131, 143].

In the most frequently used geometry, rectangular shaped $3 \times 5\,\mathrm{mm}^2$ size samples with an edge oriented parallel to one of the reflection planes have been studied. The latter can in most cases be naturally obtained by cleaving the sample. Several pairs of contacts, being needed for electrical measurements, are made in the middle of the edges and corners of the squared sample. Although this geometry of contacts is sufficient for study of SIA/BIA anisotropy, the results accuracy can be increased by using a larger number of contact pads forming a circle [58, 131]. The photocurrent $\boldsymbol{J}(\theta)$, where θ is the polar angle, is measured in unbiased structures via the voltage drop across a $50\,\Omega$ load resistor with a fast storage oscilloscope or applying standard lock-in technique [28]. We note that a pure optical method to measure photogalvanic currents, which provides a unique access to characterization of SIA/BIA in a contactless way, has been developed [61, 175, 180, 181]. It is based on the terahertz emission resulting from the photogalvanic currents generated by picosecond pulses of near infrared radiation. The physical principle is just the same as of the Auston switch [182, 183] used for generation of THz radiation in the terahertz time-domain spectroscopy [81, 176, 177].

5 Interplay of BIA and SIA in (001)-, (110)-, and (111)-grown III–V 2D systems

5.1 Tuning of structure inversion asymmetry by the δ-doping position In this section, we discuss the influence of the δ-doping position, quantum well width and growth conditions on SIA and BIA in III–V semiconductors based (001)-oriented quantum well structures. We begin with MPGE investigations of Si-δ-doped n-type $GaAs/Al_{0.3}Ga_{0.7}As$ structures grown by molecular-beam epitaxy at typical temperatures in excess of 600 °C. The insets in Fig. 7 sketch the conduction band edges of different QW structures together with the corresponding δ-doping position. All QWs have the same width of 15 nm but differ essentially in their doping profile. The degree of the doping asymmetry can be conveniently described by the parameter

$$\chi = \frac{l - r}{l + r},$$

where l and r are the spacer layer thicknesses between QW and δ-layers. Variation of individual BIA and SIA contributions as well as their ratio have been studied applying magneto-gyrotropic photogalvanic effect [60]. In these experiments, unpolarized terahertz radiation at normal incidence was used for excitation of QW structure subjected to

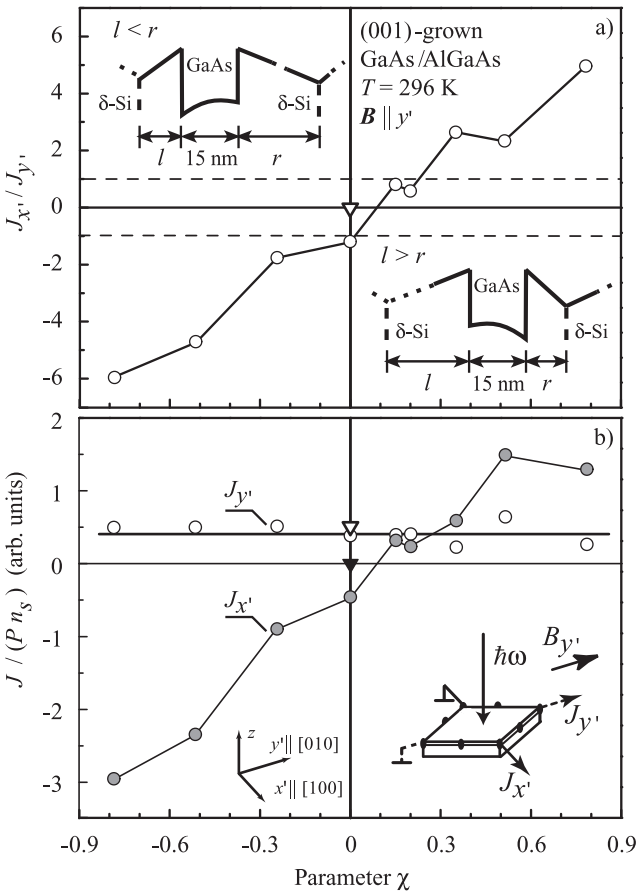

Figure 7 (a) The ratio of the SIA and BIA contributions to the MPGE, $J_{x'}/J_{y'}$, as a function of χ. The triangles show the result for sample grown at $T_\delta = 490\,^\circ\mathrm{C}$, the circles demonstrate the data for all other samples grown at $T_\delta \approx 630\,^\circ\mathrm{C}$. Insets show the QW profile and the doping positions for $l < r$ and for $l > r$. (b) Dependence of J/Pn_s on the parameter χ, here n_s is the carrier density, and P is the radiation power. The photocurrents $J_{y'}$ and $J_{x'}$ are measured along and normal to $\boldsymbol{B} \parallel y'$. Full and open symbols show J_x and J_y, respectively (triangles are the data for sample fabricated with reduced temperature during the δ-doping ($T_\delta = 490\,^\circ\mathrm{C}$)). Inset shows experimental geometry. After [60].

an in-plane magnetic field applied along a cubic axis y'. BIA and SIA photocurrent contributions have been obtained by measuring the current along and perpendicular to the magnetic field, i.e., $J_{y'}$ and $J_{x'}$, respectively. The ratio of SIA/BIA contribution as a function of the parameter χ is shown in Fig. 7a demonstrating that it has a strong dependence on the doping position and, moreover, changes its sign for $\chi \approx 0.1$. The analysis of the individual contributions shown in Fig. 7b indicates that in all structures BIA remains almost unchanged and the SIA is solely responsible for the variation of the band spin splitting with the parameter χ.

The variation of the parameter χ shows that SIA is very sensitive to the impurity potential and its magnitude and the sign can be controlled by the δ-doping position. The fact that in nominally symmetric QWs with $\chi = 0$ SIA yields a substantial photocurrent signal reflects the dopant migration along the growth direction (segregation) during molecular beam epitaxial growth. This conclusion is supported by the MPGE measurements in symmetrically doped sample ($\chi = 0$) fabricated with reduced temperature during the δ-doping ($T_\delta = 490\,^\circ$C). At this conditions segregation is suppressed and SIA vanishes, see Fig. 7.

Investigation of the structures with different band profile and δ-doping positions show that the largest value of the SIA/BIA ratio is obtained in a single heterojunction [59]. While optical experiments on spin relaxation in undoped samples demonstrate that the variation of the band profile does not substantially affect SIA [70, 71] in doped structures it seems to play an important role. Indeed in structures with strongly asymmetric potential profile like triangular confinement potential or stepped QWs, the electron function is shifted to one of the interfaces and is strongly affected by the impurity Coulomb potential [184]. The second reason for the enlarged SIA/BIA ratio in wide 2D structures is the decrease of the Dresselhaus SOI, which is given by the size quantization of the electron wave vector k_z along the growth direction z. Theory shows that BIA for a QW of width L_w should change after $\langle k_z^2 \rangle \propto 1/L_w^2$ [2]. This behavior was experimentally confirmed by optical monitoring of the angular dependence of the electron spin precession on the direction of electron motion with respect to the crystallographic axes [188, 189]. The latter has been obtained driving a current through the structure. A set of (001)-grown GaAs/AlGaAs QWs with different well widths between 6 and 30 nm and fixed parameter χ have been studied demonstrating a linear increase of the Dresselhaus splitting with the increase of the confinement parameter $\langle k_z^2 \rangle$. The linear fit presented in Fig. 8 yields the bulk Dresselhaus coefficient, cf. Eq. (1), for GaAs, $\gamma = (-11 \pm 2)\,\text{eV}\,\text{Å}^3$. The data also allowed to measure the cubic in $\boldsymbol{k}$ Dreeselhaus term showing that in GaAs it is substantially smaller than the linear one (from 2 up to 30 times, for 3 and 6 nm QWs, respectively).

The experiments on the optical monitoring of the spin precession as a function of L_w also provided information on the sign of the g^*-factor confirming its sign change at $L_w = 7$ nm [188]. This inversion is mostly caused by the opposite signs of the g^*-factor in the GaAs with respect to the

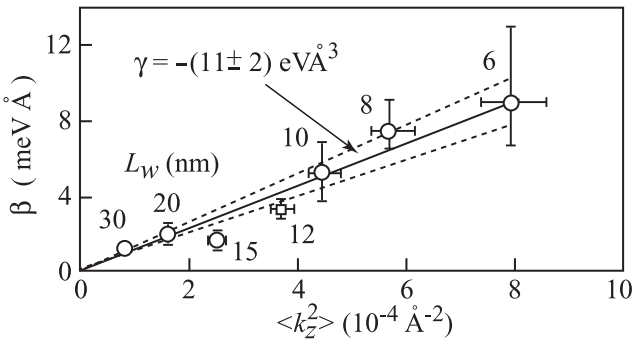

Figure 8 Measured linear in $\boldsymbol{k}$ BIA spin splitting, β, versus $\langle k_z^2 \rangle$. Circles and square are the data of Refs. [188] and [189], respectively. Solid line is the fit to $-\gamma \langle k_z^2 \rangle$ and dotted lines are 95% confidence interval. Error bars show the estimated uncertainty in the fitted slope. Horizontal bars depict ±0.5 nm variation in L_w and vertical bars indicate 30% variation in carrier density. After [188].

AlGaAs barrier and the fact that for narrow QWs the electron wave function deeply penetrates into the barrier [190–194]. The change of sign is of particular importance for the studies of the magneto-photogalvanic effects resulting from the spin-related roots. As discussed above, the MPGE photocurrent is proportional to the Zeeman band spin splitting and is determined by the effective Landé factor g^*. The same set of samples as that investigated in the work of Walser et al. [188] was previously used to provide an experimental evidence for spin-related roots of the current formation in most of (001) GaAs QWs at room temperature [195]. Figure 9 shows the MPGE photocurrent $\boldsymbol{J}^{\text{L}}$ as a function of L_w. For comparison, g^* extracted from the time-resolved Kerr rotation is also plotted. As an important result, Fig. 9 demonstrates that the photocurrent, similarly to the g^*-factor, changes its sign upon the variation of L_w. However, there is a difference in the zero points: While the $g^* = 0$ at $L_w = 7$ nm, the current vanishes for $L_w \approx 10$ nm. A small current detected at g^* inversion point, at which spin mechanism of MPGE is disabled, is caused by the orbital mechanism [195, 196], which is almost independent on L_w. For other QW widths, the spin related mechanism dominates the total current. The dominating contribution of spin mechanisms in GaAs QWs is also demonstrated for the circular MPGE [195], where in-plane spin density required for spin-galvanic effect is created via optical excitation and the Hanle effect [59, 126].

Circular photogalvanic and spin galvanic effects have also been applied for studying the SIA/BIA-ratio in (001)-oriented doped InAs/InGaSb QWs and InGaAs/InAlAs QW structures [58, 59]. In InAs/InGaSb QWs, the measurements yield the value in the range 1.6–2.3, which agrees well with theoretical results [197] predicting a dominating Rashba spin–orbit coupling for InAs QWs and is also consistent with experiments applying other transport methods [50, 198]. Note that the Rashba term is very sensitive to details of the sample growth and further treatment. Furthermore, photogalvanic methods have been applied to study the SIA/BIA-ratio in a set of InGaAs/InAlAs QW structures with semitrans-

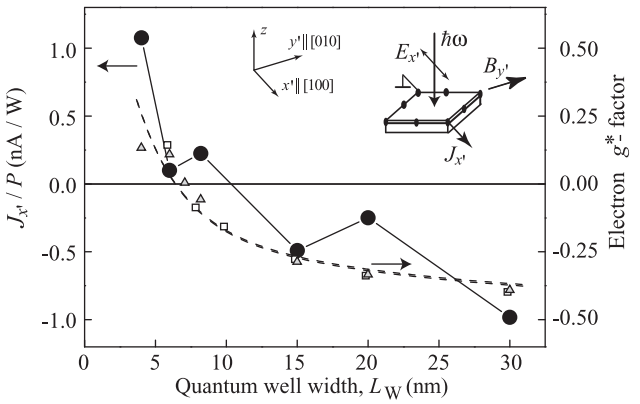

Figure 9 Dependence of the MPGE (circles) on L_w obtained at room temperature, $B_y = \pm 1$ T and photon energy $\hbar\omega = 4.4$ meV and corresponding g^*-factors (triangles determined by by TRKR [195] and squares by comparison of BIA and Zeeman spin splitting [188]). The inset shows the experimental geometry. After [195].

parent gate [131]. The measurements supported by the WAL experiments permitted to find a proper QW design for the realization of the persistent helix conditions. These results are discussed in Section 5.2.

To complete the picture, we note that BIA and SIA induced CPGE, SGE, and MPGE have been also observed in (001)-oriented InSb/(Al,In)Sb and HgTe/CdHgTe quantum well structures [65, 199–202]. These narrow band materials are of particular interest for spin physics because they are characterized by high mobility and small effective masses as well as by a very large g^*-factor and spin–orbit splitting [203–207]. So far, while confirmed the band spin splitting, most of the studies have been aimed to the mechanisms of the current formation in these novel materials, which can now be extended by special studies aimed to SIA/BIA interplay.

The experiments described above were carried out applying terahertz/microwave radiation. The dominant mechanism of the spin–orbit splitting, however, can also be determined from study of photogalvanics caused by interband absorption [208–210]. An interesting possibility to study the spin splitting provides the study of the CPGE spectra [130, 208]: the SIA-induced CPGE photocurrent has a spectral sign inversion in contrast to the BIA-one. The interplay of the Rashba/Dresselhaus has been investigated in applying CPGE in Ref. [66, 211–213] and MPGE in [173].

To conclude this part, the observation of the sign reversal of the Rashba/Dresselhaus-ratio upon changing the δ-doping position in the heterostructure together with quantum well width dependence of BIA can be used for growth of 2D structures with controllable spin splitting. It is important to note that measurements have also been carried out at technologically important room temperature at which other methods based on spin-relaxation or antilocalization experiments can not be applied. Thus, the measurements of photogalvanics can be used as a necessary feedback for technologists looking for perfectly symmetric structures with zero Rashba constant or for structures with equal Rashba and Dresselhaus spin-splittings. The latter will be discussed in the next section.

5.2 Quantum well design requirements for long spin relaxation times in (001)-grown QWs and realization of persistent spin helix The strongest anisotropy of the spin–orbit splitting can be achieved in zinc-blende semiconductor-based (001)-grown QWs with the $\boldsymbol{k}$-linear Rashba and Dresselhaus terms of equal strength, $\alpha = \beta$. Under these circumstances and for unessential contribution of $\boldsymbol{k}$-cubic BIA terms, the spin splitting vanishes in certain $\boldsymbol{k}$-space direction. Moreover, the resulting effective magnetic field $\boldsymbol{B}_{\rm eff}(\boldsymbol{k})$ is aligned along one of the $\langle 110\rangle$ crystallographic axes for any wavevector $\boldsymbol{k}$, see Fig. 2g. Consequently, it becomes ineffective for spins oriented along this axis. In this particular case, the interference of the Dresselhaus and Rashba terms leads to the (i) disappearance of an anti-localization [49, 50]) suppression of the Dyakonov–Perel relaxation for spin oriented along $\boldsymbol{B}_{\rm eff}$ [21–23], (ii) lack of SdH beating [214, 215], and (iii) makes possible the formation of the PSH. The latter represents a new state of such a spin–orbit coupled system, which was predicted in Ref. [25] and experimentally observed in GaAs 2DES with weak $\boldsymbol{k}$-cubic Dresselhaus terms (see, e.g., [216]) applying transient spin-gating spectroscopy [26, 27]. In this particular case, spin precession around the fixed axis $\boldsymbol{B}_{\rm eff} \parallel [1\bar{1}0]$ supports the space oscillations of the spin distribution in the [110] direction with a period $\pi\hbar^2/(2m^*\alpha)$. Indeed, the precession angle for electron spins aligned in the $(1\bar{1}0)$ plane equals to 2π after passing each period, while the spins oriented along $[1\bar{1}0]$ direction are intact at all. This demonstrates the stability of the space oscillating state (PSH state) to the spin precession. The specific spin splitting for $\alpha = \beta$ serving novel ways for spin manipulation attracted valuable attention. There has been much effort in this field both theoretically with new device proposals [24, 46] and discussion of the PSH formation [217–222] as well as experimentally with the aim to obtain SIA equal to BIA [26, 27, 55–58, 60, 131].

The design and growth of structures with a defined SIA/BIA-ratio needs techniques for its control. Generally, the requirement of $\alpha = \beta$ can be fulfilled by the variation of both Rashba and Dresselhaus terms, which depend on a number of macroscopic parameters, such as material of quantum well, quantum well width, doping profile and growth temperature, gate voltage, carrier density, sample temperature, etc. The Dresselhaus SOI is primary determined by the material properties and quantum well width and is fixed for a given quantum well [223]. Therefore, the only way to realize $\alpha = \beta$ in a given QW is to control the Rashba term. The latter can be achieved by the position of the asymmetric δ-doping [26, 60, 131], see Section 5.1, or by the application of a gate voltage [131, 198, 224–226]. Figure 7a shows that in 15 nm wide GaAs QWs the $\alpha = \pm\beta$ condition is achieved for $\chi = 0$ and $\chi \approx 0.17$. In these structures, the ratio of the BIA and SIA related photocurrents $|J_{x'}/J_{y'}|$ is

about unity indicating that SIA and BIA have almost equal strengths. Consequently, one obtains the spin splitting cancellation either in $[1\bar{1}0]$ or [110] crystallographic direction depending on the relative sign of the SIA and BIA terms.

While the weak $\boldsymbol{k}$-cubic SOI in GaAs based QWs barely affects the PSH formation, the important question arises whether a PSH type state will generally survive in materials with strong SOI where finite $\boldsymbol{k}$-cubic terms gain importance, in particular for heterostructures at higher charge carrier densities. The effect of cubic in $\boldsymbol{k}$ terms on PSH has been analyzed in a few theoretical works [49, 50, 158, 227–230] and has been demonstrated experimentally in Ref. [131]. The PSH conditions and the influence of the cubic in $\boldsymbol{k}$-terms on spin transport in a material with strong SOI have been studied in InGaAs QWs applying two complementary experiments, transport and photogalvanics [131]. In this work strain-free (001)-grown $In_{0.53}Ga_{0.47}As/In_{0.52}Al_{0.48}As$ quantum well structures hosting a two-dimensional electron gas were designed to achieve almost equal linear Rashba and Dresselhaus coefficients, α and β, at zero gate voltage. Since β is usually much smaller than α in InGaAs 2DEGs [231], one needed to enhance β and to reduce the built-in Rashba SOI. The former condition was achieved by making use the dependence of the Dresselhaus term on the QW widths, $\beta \propto 1/L_w^2$, and growing sufficiently narrow QWs of width $L_w = 4$ and 7 nm. A small α at zero gate bias was obtained by preparing symmetric InGaAs QWs. For that two Si doping layers with densities $n_1 = 1.2$ and $n_2 = 3.2 \times 10^{18}$ cm^{-3} were placed into the InAlAs barriers, each 6 nm away from the QW. Here, the higher doping level on the top side of the QW compensates the surface charges. A fine tuning of the Rashba spin splitting was achieved by the gate voltage.

Figure 10 shows experimental geometry and the anisotropy of the spin-galvanic signal. The current is studied in 4 nm QW at room temperature applying radiation with wavelength 148 μm. It is measured along different in-plane directions determined by the azimuth angle θ with respect to the fixed in-plane magnetic field $\boldsymbol{B} \parallel x$. The current component, J_R, parallel to the magnetic field is driven by the Rashba spin splitting, while the perpendicular component, J_D is caused by the Dresselhaus SOI, see Section 3. The data can be well fitted by $J = J_R \cos\theta + J_D \sin\theta$, with $J_R/J_D = 0.98 \pm 0.08$. This ratio is related to that between the linear Rashba and Dresselhaus SOI strengths, $J_R/J_D = \alpha/\tilde{\beta}$. The renormalized coefficient $\tilde{\beta}$ is described by Eq. (10) and takes into account the influence of the first harmonic of the cubic in $\boldsymbol{k}$ spin–orbit terms on linear in $\boldsymbol{k}$ band spin splitting, see Section 2.1. The results of Fig. 10c demonstrate that in ungated 4 nm QW samples the condition of the PSH creation is fulfilled. The $\alpha = \tilde{\beta}$ condition indicating the cancellation of the linear in $\boldsymbol{k}$ SOI has been also verified applying CPGE technique, see Section 3. By contrast, for the 7 nm QW with smaller β a substantially stronger SIA, $\alpha/\tilde{\beta} \approx 4$, has been measured applying both techniques. SGE and CPGE measurements carried out at low temperatures $T \approx 5$ K demonstrated a weak temperature dependence of α/β. The fact that the ratio of these spin–orbit constants

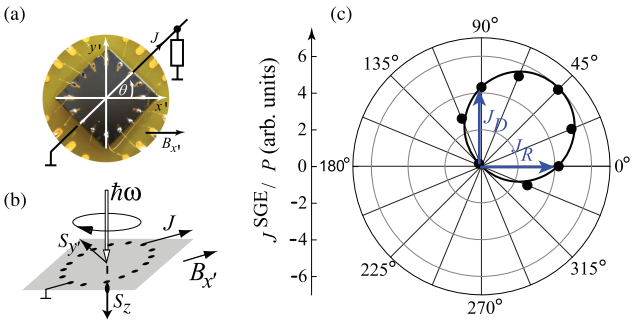

Figure 10 (a) Sample geometry and (b) sketch of the experimental arrangement used for measurements of the spin-galvanic effect in InGaAs quantum wells. For these measurements, the samples were irradiated by circularly polarized light along the growth direction, and an external magnetic field was applied along the x'-axis. The light generates a nonequilibrium spin polarization $\boldsymbol{S} \parallel z$ which, by means of the in-plane magnetic field, is rotated into the QW plane resulting in $S_{y'}$. Such a nonequilibrium in-plane spin polarization causes a spin-galvanic effect [58, 126]. The photocurrent $J^{SGE}(\theta)$ is mapped by measuring successively signals from opposite contact pairs. (c) Azimuthal dependence of the SGE current $J^{SGE}(\theta)$ measured in a 4 nm QW at room temperature, $\lambda = 148$ μm and $B_x = 0.8$ T. The solid line shows the fit according to $J = J_R \cos\theta + J_D \sin\theta$ with the ratio of $J_R/J_D = 0.98 \pm 0.08$. After [131].

is almost independent of temperature in studied InAs QWs is in agreement with the theory. Owing to a small electron effective mass (around $0.04m_0$) and a high electron density ($n_s = 3.5 \times 10^{12}$ cm^{-2}), the Fermi energy is about 170 meV. This means that the 2D electron gas is degenerate even at room temperature. The temperature-dependent corrections to the Rashba and Dresselhaus constants are in the order of the ratio of the thermal energy to the Fermi energy which is less then 15% in the studied structure even at room temperature.

The SIA/BIA cancellation in 4 nm QWs has also been obtained in transport experiment where the quantum correction to the magneto-conductivity in the gated Hall bar structures was measured in the presence of an external magnetic field $\boldsymbol{B}$, pointing perpendicularly to the QW plane, see Ref. [232]. Figures 11a and b show the measured magneto-conductance profiles at different gate voltages for the 4 and 7 nm wide QWs, respectively. On the one hand, for the 7 nm QW, only WAL characteristics are observed, which get enhanced with increasing N_s. On the other hand, most notably, the magneto-conductance for the 4 nm QW near $B = 0$ changes from WAL to weak localization (WL) characteristics and back again to WAL upon increasing N_s from 3.23 to 4.23×10^{12} cm^{-2}. The occurrence of WL (at $N_s = 3.71 \times 10^{12}$ cm^{-2}) reflects suppressed spin relaxation, and the observed sequence WAL-WL-WAL unambiguously indicates that – even in presence of strong $\boldsymbol{k}$-cubic SOI – a PSH condition is fulfilled in the WL region.

Comparison of the photocurrent measurements with the weak localization experiments enables us to extract information on the role of the cubic terms. Indeed, while the photocurrent experiments are insensitive to the third har-

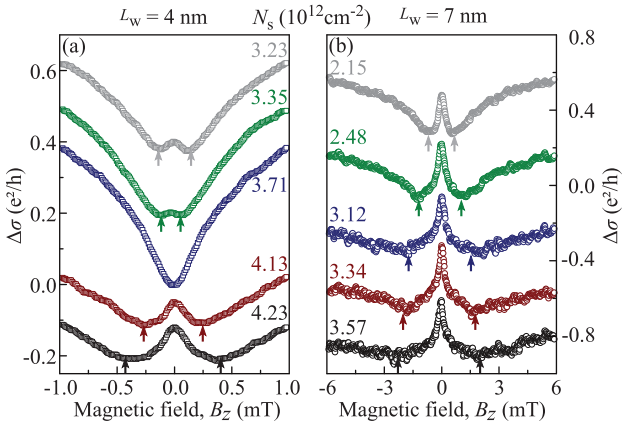

Figure 11 Magneto-conductance profiles (in units of e^2/h) measured at different gate voltages, i.e., carrier densities N_s, for (a) 4 and (b) 7 nm QWs InGaAs quantum wells at $T = 1.4$ K. All curves in (a) and (b) are shifted positively (gray and green) and negatively (black and red) with respect to the blue curve, for which $\Delta\sigma = 0$ at $B_z = 0$ mT. For the 4 nm QW, a clear WL dip occurs for a carrier density of 3.71×10^{11} cm^{-2}, which is absent for the 7 nm QW. After [131].

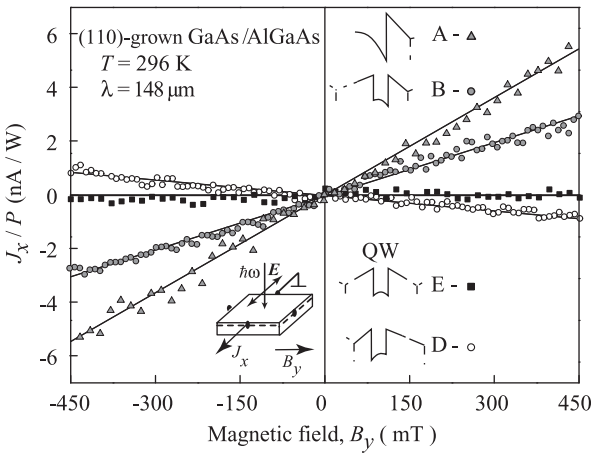

Figure 12 Magnetic field dependences of the photocurrents measured in x-direction for the radiation polarized along x and the in-plane magnetic field $\boldsymbol{B} \parallel y$. The left inset shows the experimental geometry. Four right insets show the band profile and the δ-doping position of the investigated samples. After [33].

monic of the cubic term $\boldsymbol{B}_{\rm eff}^{(3)}(\boldsymbol{k})$, and thus reveal only the ratio $\alpha/\tilde{\beta}$, the transport experiment probes spin randomization due to the entire SOI contribution, Eqs. (2), (3), and (7). A numerical analysis of the WAL-WL-WAL transition applying $\alpha/\tilde{\beta}$ obtained from the photocurrent data clearly demonstrated that a PSH type state remains even for finite cubic SOI. The essential prerequisite for this is that α and β are close to each other, a condition which for InAs-based structures can be reached in very narrow and almost symmetric QWs due to a specially designed doping profile. However, in contrast to systems with dominating $\boldsymbol{k}$-linear spin splitting, the PSH is obtained for close, but nonequal Rashba and Dresselhaus strengths.

5.3 Symmetry and spin dephasing in (110)-grown quantum wells Quantum well structures prepared on (110)-oriented GaAs substrates are of particular interest because in QWs of this orientation and special design extraordinarily slow spin dephasing can be achieved. Spin lifetimes up to several nanoseconds [29–33, 35, 36, 233–245] or even submicroseconds [38] have been reported in GaAs and other III–V semiconductor-based heterostructures, for review see, e.g., [16]. As discussed in Section 2.2, in structures of this orientation the effective magnetic field induced by the BIA points along the growth axis and does not lead to the Dyakonov–Perel relaxation of spins oriented along this direction. Therefore, in symmetrical (110)-grown QWs with SOI solely determined by BIA, spin relaxation of the z-component is governed by the Elliott–Yafet mechanism (see, e.g., [22]) being rather ineffective in GaAs based QWs. However, in asymmetric QWs this advantage fades away due to the Dyakonov–Perel spin relaxation caused by Rashba spin splitting. In undoped samples, this condition seems to be naturally fulfilled, as demonstrated by time- and polarization-resolved transmission measurements in Ref. [29], where long spin lifetimes were found. However, in doped QW samples SIA is strongly affected by the impurity Coulomb potential and growth of symmetrical QWs with negligible SIA becomes a challenging task. Discussion of this and other external factors limiting the spin relaxation time have been the subject of a large number of theoretical works, see, e.g., [101–103, 246–251].

The degree of the SIA has been analyzed in a set of double side δ-doped QW samples with different parameter χ applying MPGE, see Section 3. The degree of SIA is reflected in the magnetic field dependence of the photocurrent displayed in Fig. 12. From the symmetry arguments addressed in Sections 2.2 and 3, it follows that for *in-plane* magnetic field used for this measurements the MPGE current $J_x^{\rm MPGE}(B_y)$ is determined solely by SIA and, consequently, becomes possible only in the case of nonzero Rashba spin splitting. In line with these arguments, we obtained that the slope of $J_x^{\rm MPGE}(B_y)$ reverses upon variation of the parameter χ from positive to negative values. As an important result of these measurements, the zero current response, i.e., zero SIA, is obtained for the almost symmetrically doped QWs, $\chi = 0$, grown at 480 °C [33, 252]. This is in contrast to (001)-oriented structures grown under standard conditions ($T > 600$ °C) where for QWs with $\chi = 0$ a substantial SIA is detected, see Section 5.1 and Fig. 7. This essential difference stems from the growth temperature, and, subsequently, the impurity segregation length. While for *in-plane* magnetic field only SIA related MPGE is possible, for an *out-of-plane* magnetic field B_z the BIA related photocurrent is allowed and indeed observed for all samples. The latter demonstrate that for the structures with $\chi \neq 0$ SIA becomes important and, as demonstrated by complimentary TRKR experiments, spin relaxation accelerates. Note that studies of photocurrents

excited in (110)-grown QW structures in the absence of an external magnetic field [61, 253–256] are consistent with the results on MPGE and TRKR.

Study of spin relaxation in the QW structure characterized by photogalvanic measurements and other double side δ-doped QWs confirmed that in structures with symmetric doping ($\chi = 0$) the spin relaxation time is maximal. In these strutures, the spin dephasing has been investigated applying time- and polarization-resolved photoluminescence (TRPL) [31, 33, 252], spin noise spectroscopy [34–36]. The measurements yield the record values of the spin dephasing times in GaAs up to 250 ns were obtained applying resonant spin amplification technique [38] and demonstrate that symmetrically doped (110)-oriented QW structures set the upper limit of spin dephasing in GaAs QWs.

6 Interplay of BIA and SIA in other 2D systems

6.1 Structure inversion asymmetry and spin splitting in wurtzite QWs Wurtzite low-dimensional structures, in particular wide bandgap GaN, has been extensively investigated for applications as blue and ultraviolet light sources [257] as well as for high temperature and high power electronic devices [258–260]. The commercial fabrication of blue and green LEDs has led to well-established technological procedures of epitaxial GaN preparation and sparked a great research activity on the properties of heterostructures based on GaN and its alloys with AlN and InN. Two-dimensional GaN also attracted growing attention as a potentially interesting material system for spin physics since, doped with manganese, it is expected to become ferromagnetic with a Curie-temperature above room temperature [261]; being gadolinium doped it may offer an opportunity for fabricating magnetic semiconductors [262–266]; and GaN-based structures show rather long spin relaxation times [267–269]. A further important issue is the existence of considerable Rashba spin-splitting in the band structure. First indications of substantial spin–orbit splitting came from the observation of the SIA-type CPGE in GaN heterojunctions at Drude absorption of THz radiation [270]. Figure 13 shows the photocurrent as a function of the phase angle φ defining the radiation helicity. A finger print of the CPGE – reversing of the current direction upon switching helicity from right to left handed circularly polarized light – is clearly detected. The observed CPGE current always flows perpendicular to the incidence plane and its magnitude does not change upon rotation of the in-plane component of the light propagation unit vector $\hat{\boldsymbol{e}}$. The reason of this axial isotropy is that in wurtzite type structures both, SIA and BIA, lead to the same form of SOI given by Eq. (17), see Section 2.5. Therefore, they cause the linear coupling between orthogonal vectors (here photocurrent $\boldsymbol{j}$ and pseudovector $P_{\rm circ}\hat{\boldsymbol{e}}$) only. The band spin-splitting, which is actually not expected in wide band-gap semiconductors, in GaN/AlGaN heterostructures is caused by a large piezoelectric effect [271] yielding a strong electric field at the GaN/AlGaN interface. This electric field causes a polarization induced doping effect [272], and, on the other hand, results in a sizable Rashba contribution to the band spin-splitting. Making use of intraband, intersubband and interband absorption, the investigations of photogalvanic phenomena were extended to GaN QWs of various design as well as to low-dimensional wurtzite structures under uniaxial strain, demonstrating the Rashba character of the spin splitting [63, 64, 166, 167, 172, 270, 273–277]. The values of the spin splitting, up to 1 meV at the Fermi wavevector, have been obtained by magneto-transport measurements [278–282]. This results also confirmed that spin splitting is dominated by the $\boldsymbol{k}$-linear terms and the $\boldsymbol{k}$-cubic contribution is negligible. Note that studies on photogalvanic effects in InN- and ZnO-heterostructures demonstrated substantial band spin splitting also in these wurtzite materials [174, 283–286].

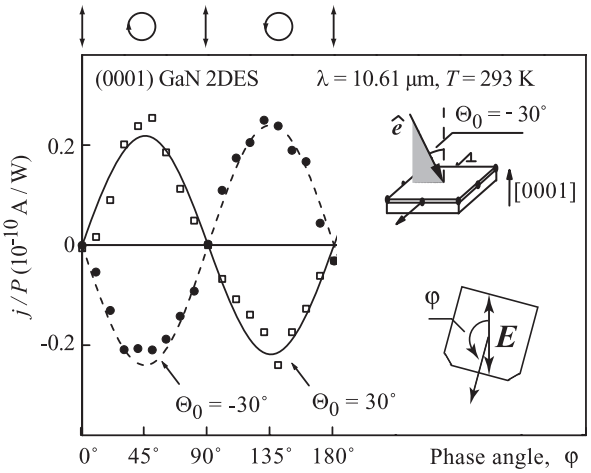

Figure 13 Photocurrent in GaN QWs normalized by the radiation power P as a function of the phase angle φ defining helicity. Measurements are presented for room temperature and irradiation by light of Q-switched CO_2 laser at the wavelength λ = 10.61 μm. The current j_x is measured for direction perpendicular to propagation of light (angle of incidence $\Theta_0 = 30^\circ$). Solid and dashed lines show calculated CPGE photocurrent. Insets sketch the experimental geometry and rotation of the $\lambda/4$-polarized by the angle φ in respect to linearly polarized laser radiation field, $\boldsymbol{E}$. The ellipses on top of the panel illustrate the polarization states for several angles φ. After [270].

6.2 Structure inversion asymmetry and spin splitting in SiGe QWs Experimental evidence of the spin degeneracy removal was in focus of the first work on photogalvanics in SiGe QWs [116]. Experiments on doped structures of various design demonstrated that SIA is the necessary prerequisite for the band spin splitting and generation of CPGE. SIA is obtained by asymmetric doping, see Fig. 14a, and/or using of stepped potential, see Fig. 14b. CPGE is detected for both systems but was absent in the symmetric QWs depicted in Fig. 14c. Examples of the photocurrent's helicity dependence are shown in Fig. 14d and e for structures grown on (001)- and (113)-oriented substrates, respectively. The measurements confirm that for (001)-grown QWs CPGE is generated only for oblique incident circularly

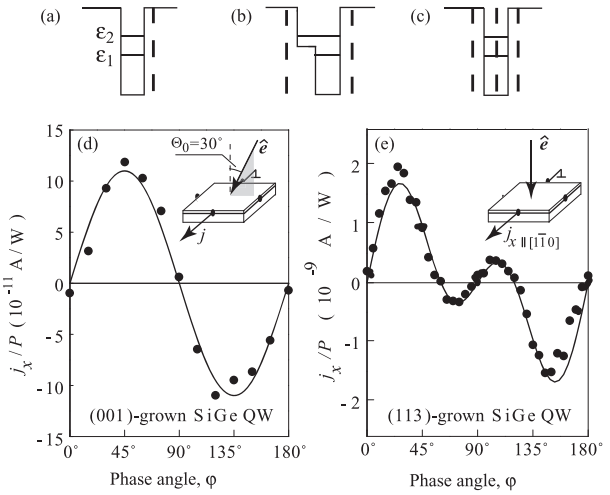

Figure 14 Potentials profiles of investigated samples: (a) asymmetrically doped compositionally symmetric QW, (b) compositionally stepped QW, and (c) symmetric QW. The vertical dashed lines indicate the doping. (d–e) Photogalvanic current j_x normalized by the light power P and measured at room temperature as a function of the phase angle φ. (d) Detected in (001)-grown and asymmetrically doped SiGe QWs. The data were obtained under oblique incidence $\Theta_0 = 30^\circ$ of irradiation at $\lambda = 10.61$ μm. The full line is fit to theory. (e) Detected in (113)-grown SiGe QWs. The results were obtained under normal incidence of irradiation at $\lambda = 280$ μm at room temperature. The full line is fit to theory. The insets in (d) and (e) show the corresponding experimental geometries. The ellipses on top of the panel illustrate the polarization states for several angles φ. After [116].

polarized light which provides an in-plane component of the photon angular momentum. The CPGE current flows normal to the plane of incidence and for a fixed angle of incidence its strengths remains constant for any light propagation direction. As both CPGE and band spin splitting are described by the equivalent second rank pseudo-tensors, see Section 3, this observation supports the conclusion that the band spin splitting in these structures is given by the Rashba term Eq. (3). The appearance of the CPGE in the stepped QWs does not contradict with the results of Eldridge et al. [71] demonstrating that in undoped 2D structures Rashba coefficient can be negligibly small despite huge conduction-band potential gradients, which break the inversion symmetry. In the discussed case, we deal with doped structures for which an asymmetric shape of QWs results in asymmetry of the dopant Coulomb force acting on free electrons. In line with symmetry arguments for symmetrically doped rectangle QW, no photogalvanic currents have been detected. A substantial SIA in asymmetrically doped SiGe QWs has been also confirmed by experiments on electron spin resonance [118, 287–289], magneto-gyrotropic photogalvanic effect [290] and CPGE at interband absorption [291].

In (113)-grown SiGe QWs, the photocurrent mostly comes from the normal incidence, see Fig. 14e [116]. The reason for the CPGE current excited by normally incident light is the reduction of symmetry from C_{2v} to C_s and the arguments are the same as that used for discussion of band spin splitting in (113)-oriented III–V QWs, see Section 2.4. Observation of such CPGE current with magnitudes comparable to that detected in GaAs QW structures indicates appearance of the band spin splitting for spins oriented normal to QW plane. We note that the large CPGE in (113)-grown SiGe QWs was not only applied for studying SIA/BIA interplay but has also been used for development of the all-electric detector of light Stokes parameters [292].

6.3 SIA/BIA interplay in (113)-, (112)-, (013)-oriented, and miscut (001)-grown zinc-blende structure-based 2DES and artificial symmetry reduction In the last part of the review, we briefly address the results obtained for zinc-blende structure based QWs of less spread crystallographic orientation. A specific property of (113)-, (112)-, (013)-oriented, and miscut (001)-grown zinc-blende structure based 2DES is the presence of spin splitting for spins oriented normal to the quantum well plane, see Section 2.4. These systems, apart from (013) oriented QWs, belong to C_s point group and have a mirror reflection plane m_1 normal to the QW plane, i.e., similar to the plane m_1 in asymmetric (110)-grown QWs depicted in Fig. 3c. The reduction of symmetry gives rise to CPGE at normal incidence and spin-galvanic effect for $\boldsymbol{S} \parallel z$, which are forbidden for (001)-oriented QWs. These effects have been detected in miscut MOCVD (001)-grown GaAs QWs [81, 127, 293] as well as in (113)-grown GaAs- and SiGe-based two-dimensional structures [108, 116, 128, 294, 295] yielding a helicity dependent photocurrent in the direction x perpendicular to m_1. The observation of the normally incident light induced photocurrent reflects the band spin splitting for electrons moving along x direction and allows to determine large g^*-factor of holes [294, 295].

While the CPGE at normal incidence has also been observed for (013)-oriented HgTe QWs the in-plane photocurrent direction changes depending on various macroscopic parameters, e.g., temperature [168]. This observation indicates that photocurrents as well as the band spin-splitting addressed in Section 3, may arbitrary change upon variation of QW design and experimental conditions. The reason for this behavior is that (013)-oriented QWs belong to the trivial point group C_1 lacking any symmetry operation except the identity. Hence, no preferential direction of the circular photocurrent or band spin splitting is forced by the symmetry arguments, see Section 2.4. It is important to note, that owing to strong spin–orbit coupling in HgTe-based QWs the CPGE has been observed to be about an 2 orders of magnitude larger than that in GaAs, InAs and SiGe low-dimensional structures. The large helicity-dependent photoresponse obtained in the wide range of radiation frequencies suggests HgTe QW structures are promising for detection of THz/IR radiation, in particularly, for the all-electric detection of the radiation Stokes parameters [169].

Finally, we note that the symmetry reduction and, consequently, band spin splitting can be obtained applying

strain even to bulk materials or depositing asymmetric lateral structures on the top of quantum well. The former way has been successfully used to obtain spin polarization by electric current (inverse spin galvanic effect) [62, 132–134, 136], in (001)-grown bulk InGaAs layers and GaAs membranes [135]. Strain has also been used to study photogalvanics and Rashba spin splitting in zinc-blende structures [61] and wurtzite GaN-based 2DES [273]. The measurements indicate a substantial $\boldsymbol{k}$-linear band spin splitting, which is forbidden without strain in these bulk materials. The possibility of artificial symmetry reduction and variation of BIA and SIA has also been demonstrated by photogalvanic studies of asymmetric lateral superlattices [296–300] and of structures with periodic quasi-one dimensional wires [170, 301].

7 Conclusions and outlook Physics of momentum dependent Rashba/Dresselhaus splitting of spin subbands in two-dimensional condensed matter systems has already resulted in a great variety of fascinating effects. This relativistic phenomenon caused by combined effect of atomic spin–orbit coupling and structure or bulk inversion asymmetry becomes possible in gyrotropic class of crystals and its form and strength can be strongly affected by the interplay of Rashba and Dresselhaus effects. The key issue in this interplay is the point group symmetry allowing for certain crystallographic configurations and structure design cancellation of the BIA and SIA or separation of Rashba and Dresselhaus band spin splitting. Several specific configurations may give rise to the extraordinary long spin relaxation states or PSH. An access to analysis of the SIA/BIA anisotropy even at technologically important room temperature provides investigation of several types of photocurrents belonging to the class of photogalvanic effects. These studies have been already used to demonstrate a possibility of the controllable variation of SIA by means of asymmetric delta-doping; to design (110)-grown QWs showing record spin relaxation times and (001)-oriented QWs with fulfilled persistent spin helix state condition; to explore the role of segregation and crystallographic orientation in the SIA/BIA strength and anisotropy; resulted in observation of SIA/BIA in wurtzite materials and SiGe QWs and have been applied to study exchange interaction in diluted magnetic QWs [302–304]. The fact that photogalvanic effects are very general and have been detected in a large number of various 2DES makes them a proper tool in the arsenal of methods sensitive to subtle details of SOI. Particularly prospective for the further studies seems to be the contactless determination of the photogalvanic current anisotropy by the terahertz time-domain spectroscopy based experiments. Finally, we anticipate, that the interplay of Rashba and Dresselhaus effects will continue to be a manifold important tool in spin physics of low-dimensional systems giving rise to many new exciting phenomena.

Acknowledgements We are grateful to S. N. Danilov, V. V. Belkov and C. Zoth for valuable discussions. This work was supported by DFG (SPP 1285), Linkage Grant of IB of BMBF at DLR, RFBR, POLAPHEN and Skoltech within the framework of the SkolTech/MIT Initiative.

References

[1] G. Dresselhaus, Phys. Rev. **100**, 580 (1955).
[2] M. I. D'yakonov and V. Yu. Kachorovskii, Fiz. Tekh. Poluprovodn. **20**, 178 (1986) [Sov. Phys. Semicond. **20**, 110 (1986)].
[3] E. I. Rashba, Fiz. Tverd. Tela **2**, 1224 (1960) [Sov. Phys. Solid State **2**, 1109 (1960)].
[4] Y. A. Bychkov and E. I. Rashba, Pis'ma Zh. Èksp. Teor. Fiz. **39**, 66 (1984) [JETP Lett. **39**, 78 (1984)].
[5] O. Krebs and P. Voisin, Phys. Rev. Lett. **77**, 1829 (1997).
[6] O. Krebs, W. Seidl, J. P. Andre, D. Bertho, C. Jonani, and P. Voisin, Semicond. Sci. Technol. **12**, 938 (1997).
[7] L. Vervoort and P. Voisin, Phys. Rev. B **56**, 12744 (1997).
[8] I. Zutic, J. Fabian, and S. Das-Sarma, Rev. Mod. Phys. **76**, 323 (2004).
[9] R. Winkler, Spin–Orbit Coupling Effects in Two-Dimensional Electron and Hole Systems (Springer, Berlin, 2003).
[10] S. Maekawa, Concepts in Spin Electronics (Oxford University Press, Oxford, 2006).
[11] J. Fabian, A. Matos-Abiague, C. Ertler, P. Stano, and I. Zutic, Acta Phys. Slov. **57**, 565 (2007).
[12] M. I. Dyakonov (ed.), Spin Physics in Semiconductors (Springer, Berlin, 2008).
[13] T. Dietl, D. D. Awschalom, and M. Kaminska (eds.), Spintronics (Semiconductors and Semimetals) (Academic Press, Inc., London, 2008).
[14] D. D. Awschalom, R. A. Buhrman, J. M. Daughton, S. von Molnar, and M. L. Roukes (eds.), Spin Electronics (Kluwer Acad. Publ., Dordrecht, 2009).
[15] D. D. Awschalom, D. Loss, and N. Samarth (eds.), Semiconductor Spintronics and Quantum Computation (Springer, Berlin, 2010).
[16] M. W. Wu, J. H. Jiang, and M. Q. Weng, Phys. Rep. **493**, 61 (2010).
[17] E. Y. Tsymbal and I. Zutic (eds.), Handbook of Spin Transport and Magnetism (Chapman and Hall, London, 2011).
[18] J. Xia, W. Ge, and K. Chang, Semiconductor Spintronics (World Scientific, Singapore, 2012).
[19] S. Maekawa, S. O. Valenzuela, E. Saitoh, and T. Kimura (eds.), Spin Current (Oxford University Press, Oxford, 2012).
[20] M. I. D'yakonov and V. I. Perel', Sov. Phys. Solid State **13**, 3023 (1972).
[21] N. S. Averkiev and L. E. Golub, Phys. Rev. B **60**, 15582 (1999).
[22] N. S. Averkiev, L. E. Golub, and M. Willander, J. Phys.: Condens. Matter **14**, R271 (2002).
[23] N. S. Averkiev and L. E. Golub, Semicond. Sci. Technol. **23**, 114002 (2008).
[24] J. Schliemann, J. C. Egues, and D. Loss, Phys. Rev. Lett. **90**, 146801 (2003).
[25] B. A. Bernevig, B. A. Orenstein, and S.-C. Zhang, Phys. Rev. Lett. **97**, 236601 (2006).
[26] J. D. Koralek, C. P. Weber, J. Orenstein, B. A. Bernevig, S.-C. Zhang, S. Mack, and D. D. Awschalom, Nature **458**, 610 (2009).

[27] M. P. Walser, C. Reichl, W. Wegscheider, and G. Salis, Nature Phys. **8**, 757 (2012).
[28] S. D. Ganichev and W. Prettl, J. Phys.: Condens. Matter **15**, R935 (2003).
[29] Y. Ohno, R. Terauchi, T. Adachi, F. Matsukura, and H. Ohno, Phys. Rev. Lett. **83**, 4196 (1999).
[30] O. Z. Karimov, G. H. John, R.T. Harley, W. H. Lau, M. E. Flatte, M. Henini, and R. Airey, Phys. Rev. Lett. **91**, 246601 (2003).
[31] S. Döhrmann D. Hägele, J. Rudolph, M. Bichler, D. Schuh, and M. Oestreich, Phys. Rev. Lett. **93**, 147405 (2004).
[32] K. C. Hall, K. Gündoğdu, J. L. Hicks, A. N. Kocbay, M. E. Flatte, T. F. Boggess, K. Holabird, A. Hunter, D. H. Chow, and J. J. Zinck, Appl. Phys. Lett. **86**, 202114 (2005).
[33] V. V. Bel'kov, P. Olbrich, S. A. Tarasenko, D. Schuh, W. Wegscheider, T. Korn, C. Schüller, D. Weiss, W. Prettl, and S. D. Ganichev, Phys. Rev. Lett. **100**, 176806 (2008).
[34] M. Römer, J. Hübner, and M. Oestreich, Rev. Sci. Instrum. **78**, 103903 (2007).
[35] G. M. Müller, M. Römer, D. Schuh, W. Wegscheider, J. Hübner, and M. Oestreich, Phys. Rev. Lett. **101**, 206601 (2008).
[36] G. M. Müller, M. Oestreich, M. Römer, and J. Hübner, Physica E **43**, 569 (2010).
[37] A. Balocchi, Q. H. Duong, P. Renucci, B. L. Liu, C. Fontaine, T. Amand, D. Lagarde, and X. Marie, Phys. Rev. Lett. **107**, 136604 (2011).
[38] M. Griesbeck, M. M. Glazov, E. Ya. Sherman, D. Schuh, W. Wegscheider, C. Schüller, and T. Korn, Phys. Rev. B **85**, 085313 (2012).
[39] H. Q. Ye, G. Wang, B. L. Liu, Z. W. Shi, W. X. Wang, C. Fontaine, A. Balocchi, T. Amand, D. Lagarde, P. Renucci, and X. Marie, Appl. Phys. Lett. **101**, 032104 (2012).
[40] K. Biermann, A. Hernández-Mínguez, R. Hey, and P. V. Santos, J. Appl. Phys. **112**, 083913 (2012).
[41] A. Hernández-Mínguez, K. Biermann, R. Hey, and P. V. Santos, Phys. Rev. Lett. **109**, 266602 (2012).
[42] G. Wang, A. Balocchi, D. Lagarde, C. R. Zhu, T. Amand, P. Renucci, Z. W. Shi, W. X. Wang, B. L. Liu, and X. Marie, Appl. Phys. Lett **102**, 242408 (2013).
[43] X. Cartoixa, D. Z.-Y. Ting, and Y.-C. Chang, Appl. Phys. Lett. **83**, 1462 (2003).
[44] K. C. Hall, W. H. Lau, K. Gündoğdu, M. E. Flatté, and T. F. Boggess, Appl. Phys. Lett. **83**, 2937 (2003).
[45] X. Cartoixa, D. Z. Y. Ting, and Y. C. Chang, J. Supercond. **18**, 163 (2005).
[46] Y. Kunihashi, M. Kohda, H. Sanada, H. Gotoh, T. Sogawa, and J. Nitta, Appl. Phys. Lett. **100**, 113502 (2012).
[47] B. Jusserand, D. Richards, H. Peric, and B. Etienne, Phys. Rev. Lett. **69**, 848 (1992).
[48] B. Jusserand, D. Richards, G. Allan, C. Priester, and B. Etienne, Phys. Rev. B **51**, 4707 (1995).
[49] F. G. Pikus and G. E. Pikus, Phys. Rev. B. **51**, 16928 (1995).
[50] W. Knap, C. Skierbiszewski, A. Zduniak, E. Litwin-Staszewska, D. Bertho, F. Kobbi, J. L. Robert, G. E. Pikus, F. G. Pikus, S. V. Iordanskii, V. Mosser, K. Zekentes, and Yu. B. Lyanda-Geller, Phys. Rev. B **53**, 3912 (1996).
[51] J. B. Miller, D. M. Zumbühl, C. M. Marcus, Y. B. Lyanda-Geller, D. Goldhaber-Gordon, K. Campman, and A. C. Gossard, Phys. Rev. Lett. **90**, 076807 (2003).
[52] G. Yu, N. Dai, J. H. Chu, P. J. Poole, and S. A. Studenikin, Phys. Rev. B **78**, 035304 (2008).
[53] M. M. Glazov and L. E. Golub, Semicond. Sci. Technol. **24**, 064007 (2009).
[54] G. M. Minkov, A. V. Germanenko, O. E. Rut, A. A. Sherstobitov, L. E. Golub, B. N. Zvonkov, and M. Willander, Phys. Rev. B **70**, 155323 (2004).
[55] M. Scheid, M. Kohda, Y. Kunihashi, K. Richter, and J. Nitta, Phys. Rev. Lett. **101**, 266401 (2008).
[56] M. Scheid, I. Adagideli, J. Nitta, and K. Richter, Semicond. Sci. Techol. **24**, 064005 (2009).
[57] Y. Kunihashi, M. Kohda, and J. Nitta, Phys. Rev. Lett. **102**, 226601 (2009).
[58] S. D. Ganichev, V. V. Bel'kov, L. E. Golub, E. L. Ivchenko, P. Schneider, S. Giglberger, J. Eroms, J. De Boeck, G. Borghs, W. Wegscheider, D. Weiss, and W. Prettl, Phys. Rev. Lett. **92**, 256601 (2004).
[59] S. Giglberger, L. E. Golub, V. V. Bel'kov, S. N. Danilov, D. Schuh, Ch. Gerl, F. Rohlfing, J. Stahl, W. Wegscheider, D. Weiss, W. Prettl, and S. D. Ganichev, Phys. Rev. B **75**, 035327 (2007).
[60] V. Lechner, L. E. Golub, P. Olbrich, S. Stachel, D. Schuh, W. Wegscheider, V. V. Bel'kov, and S. D. Ganichev, Appl. Phys. Lett. **94**, 242109 (2009).
[61] M. Bieler, N. Laman, H. M. van Driel, and A. L. Smirl, Appl. Phys. Lett. **86**, 061102 (2005).
[62] C. L. Yang, H. T. He, Lu Ding, L. J. Cui, Y. P. Zeng, J. N. Wang, and W. K. Ge, Phys. Rev. Lett. **96**, 186605 (2006).
[63] Y. O. Tang, B. Shen, H. W. He, N. Tang, W. H. C. Chen, Z. J. Yang, G. Y. Zhang, Y. H. Chen, C. G. Tang, Z. G. Wang, K. S. Cho, and Y. F. Chen, Appl. Phys. Lett. **91**, 071920 (2007).
[64] H. Zhao, B. Liu, L. Guo, C. Tan, H. Chen, and D. Chen, Appl. Phys. Lett. **91**, 252105 (2007).
[65] M. Frazier, J. A. Waugh, J. J. Heremans, M. B. Santos, X. Liu, and G. A. Khodaparast, J. Appl. Phys. **106**, 103513 (2009).
[66] J. L. Yu, Y. H. Chen, Y. Liu, C. Y. Jiang, H. Ma, and L. P. Zhu, Appl. Phys. Lett. **100**, 152110 (2012).
[67] N. S. Averkiev, L. E. Golub, A. S. Gurevich, V. P. Evtikhiev, V. P. Kochereshko, A. V. Platonov, A. S. Shkolnik, and Yu. P. Efimov, Phys. Rev. B **74**, 033305 (2006).
[68] P. S. Eldridge, W. J. H. Leyland, P. G. Lagoudakis, O. Z. Karimov, M. Henini, D. Taylor, R. T. Phillips, and R. T. Harley, Phys. Rev. B **77**, 125344 (2008).
[69] A. V. Larionov and L. E. Golub, Phys. Rev. B **78**, 033302 (2008).
[70] P. S. Eldridge, W. J. H. Leyland, P. G. Lagoudakis, R. T. Harley, R. T. Phillips, R. Winkler, M. Henini, and D. Taylor, Phys. Rev. B **82**, 045317 (2010).
[71] P. S. Eldridge, J. Hübner, S. Oertel, R. T. Harley, M. Henini, and M. Oestreich, Phys. Rev. B **83**, 041301 (2011).
[72] D. Stich, J. Zhou, T. Korn, R. Schulz, D. Schuh, W. Wegscheider, M. W. Wu, and C. Schüller, Phys. Rev. Lett. **98**, 176401 (2007).
[73] J. L. Cheng, M. W. Wu, and I. C. da Cunha Lima, Phys. Rev. B **75**, 205328 (2007).
[74] D. Stich, J. H. Jiang, T. Korn, R. Schulz, D. Schuh, W. Wegscheider, M. W. Wu, and C. Schüller, Phys. Rev. B **76**, 073309 (2007).
[75] L. Meier, G. Salis, I. Shorubalko, E. Gini, S. Schön, and K. Ensslin, Nature Phys. **3**, 640 (2007).
[76] T. Korn. D. Stich, R. Schulz, D. Schuh, W. Wegscheider, and C. Schüller, Physica E **40**, 1542 (2008).

[77] L. Meier, G. Salis, E. Gini, I. Shorubalko, and K. Ensslin, Phys. Rev. B **77**, 035305 (2008).
[78] M. Studer, S. Schön, K. Ensslin, and G. Salis, Phys. Rev. B **79**, 045302 (2009).
[79] M. Studer, M. P. Walser, S. Baer, H. Rusterholz, S. Schön, D. Schuh, W. Wegscheider, K. Ensslin, and G. Salis, Phys. Rev. B **82**, 235320 (2010).
[80] E.L. Ivchenko and S.D. Ganichev, in: Spin Physics in Semiconductors, edited by M. I. Dyakonov (Springer, Berlin, Heidelberg, 2008), pp. 245–277.
[81] S. D. Ganichev and W. Prettl, Intense Terahertz Excitation of Semiconductors (Oxford University Press, Oxford, 2006).
[82] E. L. Ivchenko and G. E. Pikus, Superlattices and Other Heterostructures. Symmetry and Optical Phenomena (Springer, Berlin, 1997).
[83] E. L. Ivchenko, Optical Spectroscopy of Semiconductor Nanostructures (Alpha Science Int., Harrow, UK, 2005).
[84] We remind that the gyrotropic point group symmetry makes no difference between certain components of polar vectors, like electric current or electron momentum, and axial vectors, like a spin or magnetic field, and is described by the gyration tensor [80, 85, 86]. Gyrotropic media are characterized by the linear in light or electron wavevector $\boldsymbol{k}$ spatial dispersion resulting in optical activity (gyrotropy) or Rashba/Dresselhaus band spin-splitting in semiconductor structures [80, 86–90], respectively. Among 21 crystal classes lacking inversion symmetry, 18 are gyrotropic, from which 11 classes are enantiomorphic (chiral) and do not possess a reflection plane or rotation-reflection axis [80, 88, 89]. Three nongyrotropic noncentrosymmetric classes are T_d, C_{3h} and D_{3h}. We note that it is often, but misleading, stated that gyrotropy (optical activity) can be obtained only in noncentrosymmetric crystals having no mirror reflection plane. In fact, seven nonenantiomorphic class groups (C_s, C_{2v}, C_{3v}, S_4, D_{2d}, C_{4v} and C_{6v}) are gyrotropic allowing addressed above linear in $\boldsymbol{k}$ spin splitting, SGE, CPGE, MPGE excited by unpolarized radiation as well as inversed SGE – spin orientation by the electric current, for review see, e.g., [91].
[85] L. D. Landau, E. M. Lifshits, and L. P. Pitaevskii, Course of Theoretical Physics, Vol. 8: Electrodynamics of Continuous Media (Elsevier, Amsterdam, 1984).
[86] J. F. Nye, Physical Properties of Crystals: Their Representation by Tensors and Matrices (Oxford Univ. Press, Oxford, 1985).
[87] V. M. Agranovich and V. L. Ginzburg, Crystal Optics with Spatial Dispersion, and Excitons, Springer Series in Solid-State Sciences Vol. 42 (Springer, Berlin, 1984).
[88] V. A. Kizel', Yu. I. Krasilov, and V. I. Burkov, Usp. Fiz. Nauk **114**, 295 (1974) [Sov. Phys. Usp. **17**, 745 (1975)].
[89] J. Jerphagnon and D. S. Chemla, J. Chem. Phys. **65**, 1522 (1976).
[90] B. Koopmans, P. V. Santos, and M. Cardona, Phys. Status Solidi B **205**, 419 (1998).
[91] S. D. Ganichev, M. Trushin, and J. Schliemann, in: Handbook of Spin Transport and Magnetism, edited by E.Y. Tsymbal and I. Zutic (Chapman and Hall, London, 2011), pp. 487–497.
[92] R. F. Tinder, Tensor Properties of Solids: Phenomenological Development of the Tensor Properties of Crystals (Morgan & Claypool Publishers, Malaysia, 2008).
[93] F. Li, Y. V. Pershin, V. A. Slipko, and N. A. Sinitsyn, Phys. Rev. Lett. **111**, 067201 (2013).
[94] Note that following to Ref. [95] a $\boldsymbol{k}$ dependent Larmor precession frequency $\Omega(\boldsymbol{k})$ of electron spin precession around $B_{\text{eff}}(\boldsymbol{k})$ is commonly used in the literature [23, 49, 95–97].
[95] G. E. Pikus and A. N. Titkov, in: Optical Orientation, edited by F. Meier and B. P. Zakharchenya (North-Holland, Amsterdam, 1984).
[96] S. V. Iordanskii, Yu. B. Lyanda-Geller, and G. E. Pikus, Pis'ma Zh. Eksp. Teor. Fiz. **60**, 199 (1994) [JETP Lett. **60**, 206 (1994)].
[97] L. E. Golub, Physics – Uspekhi **55**, 814 (2012).
[98] E. A. de Andrada e Silva, Phys. Rev. B **46**, 1921 (1992).
[99] M. A. Toloza Sandoval, A. Ferreira da Silva, E. A. Andrada e Silva, and G. C. La Rocca, Phys. Rev. B **87**, 081304(R) (2013).
[100] Note that due to combined effect of SIA and BIA in asymmetric (110) QWs an additional small term $H_{\text{SO}} = \tilde{\alpha}(\sigma_x k_y + \sigma_y k_x)$ is allowed. However, the constant $\tilde{\alpha}$ is about an order of magnitude smaller than the Rashba constant α in a rectangular QW subjected in electric field $\sim 10^5\,\text{V cm}^{-1}$ [101]. We also note that in symmetrically doped (110)-grown QWs there are spatial fluctuations of the Rashba constant yielding finite values of α which is zero in average. This spatially-fluctuating Rashba splitting leads to spin relaxation which limits the spin dephasing time in symmetrically-doped (110) QWs [102].
[101] M. O. Nestoklon, S. A. Tarasenko, J.-M. Jancu, and P. Voisin, Phys. Rev. B **85**, 205307 (2012).
[102] M. M. Glazov, E. Ya. Sherman, and V. K. Dugaev, Physica E **42**, 2157 (2010).
[103] X. Cartoixa, D. Z. Y. Ting, and Y. C. Chang, Phys. Rev. B **71**, 045313 (2005).
[104] I. Vurgaftman and J. R. Meyer, J. Appl. Phys. **97**, 053707 (2005).
[105] B. Y. Sun, P. Zhang, and M. W. Wu, J. Appl. Phys. **108**, 093709 (2010).
[106] R. Ferreira and G. Bastard, Phys. Rev. B **43**, 9687 (1991).
[107] G. Bastard and R. Ferreira, Europhys. Lett. **23**, 439 (1993).
[108] S. D. Ganichev, S. N. Danilov, V. V. Bel'kov, E. L. Ivchenko, M. Bichler, W. Wegscheider, D. Weiss, and W. Prettl, Phys. Rev. Lett. **88**, 057401 (2002).
[109] P. Schneider, J. Kainz, S. D. Ganichev, V. V. Bel'kov, S. N. Danilov, M. M. Glazov, L. E. Golub, U. Rössler, W. Wegscheider, D. Weiss, D. Schuh, and W. Prettl, J. Appl. Phys. **96**, 420 (2004).
[110] T. Korn, M. Kugler, M. Griesbeck, R. Schulz, A. Wagner, M. Hirmer, C. Gerl, D. Schuh, W. Wegscheider, and C. Schüller, New J. Phys. **12**, 043003 (2010).
[111] T. Korn, Phys. Rep. **494**, 415 (2010).
[112] M. Kugler, T. Andlauer, T. Korn, A. Wagner, S. Fehringer, R. Schulz, M. Kubová, C. Gerl, D. Schuh, W. Wegscheider, P. Vogl, and C. Schüller, Phys. Rev. B **80**, 035325 (2009).
[113] M. S. König, S. Wiedmann, C. Brüne, A. Roth, H. Buhmann, L. Molenkamp, X. L. Qi, and S. C. Zhang, Science **318**, 766 (2007).
[114] S. C. Zhang and X. L. Qi, Rev. Mod. Phys. **83**, 1057 (2011).
[115] Note that in bulk III–V semiconductors and *cubic* GaN the constant β is zero.
[116] S. D. Ganichev, U. Rössler, W. Prettl, E. L. Ivchenko, V. V. Bel'kov, R. Neumann, K. Brunner, and G. Abstreiter, Phys. Rev. B **66**, 075328 (2002).
[117] U. Rössler and J. Kainz, Solid State Commun. **121**, 313 (2002).

[118] Z. Wilamowski, W. Jantsch, H. Malissa, and U. Rössler, Phys. Rev. B **66**, 195315 (2002).
[119] L. E. Golub and E. L. Ivchenko, Phys. Rev. B **69**, 115333 (2004).
[120] M. O. Nestoklon, L. E. Golub, and E. L. Ivchenko, Phys. Rev. B **73**, 235334 (2006).
[121] M. O. Nestoklon, E. L. Ivchenko, J.-M. Jancu, and P. Voisin, Phys. Rev. B **77**, 155328 (2008).
[122] M. Prada, G. Klimek, and R. Joynt, New J. Phys. **13**, 013009 (2011).
[123] V. I. Belinicher, Phys. Lett. A **66**, 213 (1978).
[124] B. I. Sturman and V. M. Fridkin, The Photovoltaic and Photorefractive Effects in Noncentrosymmetric Materials (Gordon and Breach Science Publishers, New York, 1992).
[125] E. L. Ivchenko, Yu. B. Lyanda-Geller, and G. E. Pikus, Pis'ma Zh. Eksp. Teor. Fiz. **50**, 156 (1989) [JETP Lett. **50**, 175 (1989)].
[126] S. D. Ganichev, E. L. Ivchenko, V. V. Bel'kov, S. A. Tarasenko, M. Sollinger, D. Weiss, W. Wegscheider, and W. Prettl, Nature (London) **417**, 153 (2002).
[127] S. D. Ganichev, E. L. Ivchenko, S. N. Danilov, J. Eroms, W. Wegscheider, D. Weiss, and W. Prettl, Phys. Rev. Lett. **86**, 4358 (2001).
[128] S. D. Ganichev, E. L. Ivchenko, and W. Prettl, Physica E **14**, 166 (2002).
[129] V. V. Bel'kov, S. D. Ganichev, E. L. Ivchenko, S. A. Tarasenko, W. Weber, S. Giglberger, M. Olteanu, H.-P. Tranitz, S. N. Danilov, P. Schneider, W. Wegscheider, D. Weiss, and W. Prettl, J. Phys.: Condens. Matter **17**, 3405 (2005).
[130] L. E. Golub, Phys. Rev. B **67**, 235320 (2003).
[131] M. Kohda, V. Lechner, Y. Kunihashi, T. Dollinger, P. Olbrich, C. Schönhuber, I. Caspers, V. V. Bel'kov, L. E. Golub, D. Weiss, K. Richter, J. Nitta, and S. D. Ganichev, Phys. Rev. B **86**, 081306 (R) (2012).
[132] Inversed SGE, i.e., spin orientation by electric current (for recent review see [91]), can also be used for study of BIA/SIA anisotropy. This effect, given by $S_l = \sum_m Q'_{lm} j_m$, is observed in several low dimensional systems [62, 133–137] and like SGE reflects the spin splitting anisotropy, see, e.g., [138–142].
[133] S. D. Ganichev, S. N. Danilov, Petra Schneider, V. V. Bel'kov, L. E. Golub, W. Wegscheider, D. Weiss, and W. Prettl, cond-mat/0403641 (2004), see also J. Magn. Magn. Mater. **300**, 127 (2006).
[134] A. Yu. Silov, P. A. Blajnov, J. H. Wolter, R. Hey, K. H. Ploog, and N. S. Averkiev, Appl. Phys. Lett. **85**, 5929 (2004).
[135] Y. K. Kato, R. C. Myers, A. C. Gossard, and D. D. Awschalom, Phys. Rev. Lett. **93**, 176601 (2004).
[136] V. Sih, R. C. Myers, Y. K. Kato, W. H. Lau, A. C. Gossard, and D. D. Awschalom, Nature Phys. **1**, 31 (2005).
[137] N. P. Stern, S. Ghosh, G. Xiang, M. Zhu, N. Samarth, and D. D. Awschalom, Phys. Rev. Lett. **97**, 126603 (2006).
[138] A. G. Aronov, Yu. B. Lyanda-Geller, and G. E. Pikus, JETP **100**, 973 (1991) [Sov. Phys. JETP **73**, 537 (1991)].
[139] A. V. Chaplik, M. V. Entin, and L. I. Magarill, Physica E **13**, 744 (2002).
[140] M. Trushin and J. Schliemann, Phys. Rev. B **75**, 155323 (2007).
[141] O. E. Raichev, Phys. Rev. B **75**, 205340 (2007).
[142] L. E. Golub and E. L. Ivchenko, Phys. Rev. B **84**, 115303 (2011).
[143] V. V. Bel'kov and S. D. Ganichev, Semicond. Sci. Technol. **23**, 114003 (2008).
[144] V. V. Bel'kov and S. D. Ganichev, in: Handbook of Spintronic Semiconductors, edited by W. M. Chen and I. A. Buyanova (Pan Stanford Publishing, Singapore, 2010), pp. 243–265.
[145] R. Winkler, in: Handbook of Magnetism and Advanced Magnetic Materials Vol. 5, edited by H. Kronmuller and S. Parkin (John Wiley & Sons, New York, 2007); arXiv:cond-mat/0605390.
[146] J. Karch, P. Olbrich, M. Schmalzbauer, C. Zoth, C. Brinsteiner, M. Fehrenbacher, U. Wurstbauer, M. M. Glazov, S. A. Tarasenko, E. L. Ivchenko, D. Weiss, J. Eroms, and S. D. Ganichev, Phys. Rev. Lett. **97**, 227402 (2010).
[147] R. V. Romashko, A. I. Grachev, Yu. N. Kulchin, and A. A. Kamshilin, Opt. Express **18**, 27142 (2010).
[148] J. Karch, C. Drexler, P. Olbrich, M. Fehrenbacher, M. Hirmer, M. M. Glazov, S. A. Tarasenko, E. L. Ivchenko, B. Birkner, J. Eroms, D. Weiss, R. Yakimova, S. Lara-Avila, S. Kubatkin, M. Ostler, T. Seyller, and S. D. Ganichev, Phys. Rev. Lett. **107**, 276601 (2011).
[149] P. Hosur, Phys. Rev. B **83**, 035309 (2011).
[150] Z. D. Kvon, S. N. Danilov, D. A. Kozlov, C. Zoth, N. N. Michailov, S. A. Dvoretzkii, and S. D. Ganichev, JETP Lett. **94**, 816 (2011) [Pisma ZhETP **94**, 895 (2011)].
[151] J. W. McIver, D. Hsieh, H. Steinberg, P. Jarillo-Herrero, and N. Gedik, Nature Nanotechnol. **7**, 96 (2012).
[152] B. Dora, J. Cayssol, F. Simon, and R. Moessner, Phys. Rev. Lett. **108**, 056602 (2012)
[153] Q. S. Wu, S. N. Zhang, Z. Fang, and X. Dai, Physica E **44**, 895 (2012).
[154] C. Drexler, S. A. Tarasenko, P. Olbrich, J. Karch, M. Hirmer, F. Müller, M. Gmitra, J. Fabian, R. Yakimova, S. Lara-Avila, S. Kubatkin, and S. D. Ganichev, Nature Nanotechnol. **8**, 104 (2013).
[155] P. Olbrich, C. Zoth, P. Vierling, K.-M. Dantscher, G. V. Budkin, S. A. Tarasenko, V. V. Bel'kov, D. A. Kozlov, Z. D. Kvon, N. N. Mikhailov, S. A. Dvoretsky, and S. D. Ganichev, Phys. Rev. B **87**, 235439 (2013).
[156] S. N. Artemenko and V. O. Kaladzhyan, JETP Lett. **97**, 82 (2013).
[157] A. Łusakowski, J. Wróbel, and T. Dietl, Phys. Rev. B **68**, R081201 (2003).
[158] S. Kettemann, Phys. Rev. Lett. **98**, 176808 (2007).
[159] W. H. Lau and M. E. Flatté, Phys. Rev. B **72**, R161311 (2005).
[160] S. D. Ganichev, J. Diener, I. N. Yassievich, W. Prettl, B. K. Meyer, and K. W. Benz, Phys. Rev. Lett. **75**, 1590 (1995).
[161] E. Ziemann, S. D. Ganichev, I. N. Yassievich, V. I. Perel, and W. Prettl, J. Appl. Phys. **87**, 3843 (2000).
[162] S. D. Ganichev, I. N. Yassievich, and W. Prettl, J. Phys.: Condens. Matter **14**, R1263 (2002).
[163] Z. D. Kvon, S. N. Danilov, N. N. Mikhailov, S. A. Dvoretsky, and S. D. Ganichev, Physica E **40**, 1885 (2008).
[164] G. M. H. Knippels, X. Yan, A. M. MacLeod, W. A. Gillespie, M. Yasumoto, D. Oepts, and A. F. G. van der Meer, Phys. Rev. Lett. **83**, 1578 (1999).
[165] O. Svelto, Principles of Lasers, fifth ed. (Springer, New York, 2010).

[166] W. Weber, L. E. Golub, S. N. Danilov, J. Karch, C. Reitmaier, B. Wittmann, V. V. Bel'kov, E. L. Ivchenko, Z. D. Kvon, N. Q. Vinh, A. F. G. van der Meer, B. Murdin, and S. D. Ganichev, Phys. Rev. B **77**, 245304 (2008).
[167] B. Wittmann, L. E. Golub, S. N. Danilov, J. Karch, C. Reitmaier, Z. D. Kvon, N. Q. Vinh, A. F. G. van der Meer, B. Murdin, S. D. Ganichev, Phys. Rev. B **78**, 205435 (2008).
[168] B. Wittmann, S. N. Danilov, V. V. Bel'kov, S. A. Tarasenko, E. G. Novik, H. Buhmann, C. Brüne, L. W. Molenkamp, E. L. Ivchenko, Z. D. Kvon, N. N. Mikhailov, S. A. Dvoretsky, N. Q. Vinh, A. F. G. van der Meer, B. Murdin, and S. D. Ganichev, Semicond. Sci. Technol. **25**, 095005 (2010).
[169] S. N. Danilov, B. Wittmann, P. Olbrich, W. Eder, W. Prettl, L. E. Golub, E. V. Beregulin, Z. D. Kvon, N. N. Mikhailov, S. A. Dvoretsky, V. A. Shalygin, N. Q. Vinh, A. F. G. van der Meer, B. Murdin, and S. D. Ganichev, J. Appl. Phys. **105**, 013106 (2009).
[170] Ch. Jiang, H. Ma, J. Yu, Y. Liu, and Y. Chen, Appl. Phys. Lett. **99**, 032106 (2011).
[171] V. V. Bel'kov, S. D. Ganichev, P. Schneider, C. Back, M. Oestreich, J. Rudolph, D. Hägele, L. E. Golub, W. Wegscheider, W. Prettl, Solid State Commun. **128**, 283 (2003).
[172] K. S. Cho, Y. F. Chen, Y. Q. Tang, and B. Shen, Appl. Phys. Lett. **90**, 041909 (2007).
[173] J. Dai, H.-Z. Lu, C. L. Yang, S.-Q. Shen, F.-C. Zhang, and X. Cui, Phys. Rev. Lett. **104**, 246601 (2010).
[174] Q. Zhang, X. Q. Wang, C. M. Yin, F. Y. Xu, N. Tang, B. Shen, Y. H. Shen, K. Chang, W. K. Ge, Y. Ishitani, and A. Yoshikawa, Appl. Phys. Lett. **97**, 041907 (2010).
[175] S. Priyadarshi, K. Pierz, and M. Bieler, Appl. Phys. Lett. **102**, 112102 (2013).
[176] K. Sakai, Terahertz Optoelectronics, Topics in Applied Physics (Springer, Berlin, 2005).
[177] Y.-S. Lee, Principles of Terahertz Science and Technology (Springer, Berlin, 2009).
[178] C. Drexler, V. V. Bel'kov, B. Ashkinadze, P. Olbrich, C. Zoth, V. Lechner, Ya. V. Terent'ev, D. R. Yakovlev, G. Karczewski, T. Wojtowicz, D. Schuh, W. Wegscheider, and S. D. Ganichev, Appl. Phys. Lett. **97**, 182107 (2010).
[179] S. D. Ganichev, V. V. Bel'kov, S. A. Tarasenko, S. N. Danilov, S. Giglberger, Ch. Hoffmann, E. L. Ivchenko, D. Weiss, W. Wegscheider, Ch. Gerl, D. Schuh, J. Stahl, J. De Boeck, G. Borghs, and W. Prettl, Nature Phys. **2**, 609 (2006).
[180] D. Sun, C. Divin, J. Rioux, J. E. Sipe, C. Berger, W. A. de Heer, P. N. First, and T. B. Norris, Nano Lett. **10**, 1293 (2010).
[181] D. Sun, J. Rioux, J. E. Sipe, Y. Zou, M. T. Mihnev, C. Berger, W. A. de Heer, P. N. First, and T. B. Norris, Phys. Rev. B **85**, 165427 (2012).
[182] P. R. Smith, D. H. Auston, and M. C. Nuss, IEEE J. Quantum Electron. **QE-24**, 255 (1988).
[183] X.-C. Zhang, B. B. Hu, J. T. Darrow, and D. H. Auston, Appl. Phys. Lett. **56**, 1011 (1990).
[184] Note that the influence of QW shape on photogalvanic and magneto-photogalvanic effects have been analyzed in Refs. [185–187].
[185] K. Majchrowski, W. Pasko, and I. Tralle, Phys. Lett. A **373** 2959 (2009).
[186] K. Majchrowski, W. Pasko, and I. Tralle, Acta Phys. Polon. A **116**, 854 (2009).
[187] M. V. Entin and L. I. Magarill, JETP Lett. **97**, 639 (2013).
[188] M. P. Walser, U. Siegenthaler, V. Lechner, D. Schuh, S. D. Ganichev, W. Wegscheider, and G. Salis, Phys. Rev. B **86**, 195309 (2012).
[189] P. Walser, C. Reichl, W. Wegscheider, and G. Salis, Nature Phys. **8**, 757 (2012).
[190] M. J. Snelling, G. P. Flinn, A. S. Plaut, R. T. Harley, A. C. Tropper, R. Eccleston, and C. C. Phillips, Phys. Rev. B **44**, 11345 (1991).
[191] E. L. Ivchenko, A. A. Kiselev, and M. Willander, Solid State Commun. **102**, 375 (1997).
[192] G. Salis, Y. Kato, K. Ensslin, D. C. Driscoll, A. C. Gossard, and D. D. Awschalom, Nature **414**, 619 (2001).
[193] I. A. Yugova, A. Greilich, D. R. Yakovlev, A. A. Kiselev, M. Bayer, V. V. Petrov, Yu. K. Dolgikh, D. Reuter, and A. D. Wieck, Phys. Rev. B **75**, 245302 (2007).
[194] M. Kugler, T. Andlauer, T. Korn, A. Wagner, S. Fehringer, R. Schulz, M. Kubova, C. Gerl, D. Schuh, W. Wegscheider, P. Vogl, and C. Schüller, Phys. Rev. B **80**, 035325 (2009).
[195] V. Lechner, L. E. Golub, F. Lomakina, V. V. Bel'kov, P. Olbrich, S. Stachel, I. Caspers, M. Griesbeck, M. Kugler, M. J. Hirmer, T. Korn, C. Schüller, D. Schuh, W. Wegscheider, and S. D. Ganichev, Phys. Rev. B **83**, 155313 (2011).
[196] S. A. Tarasenko, Phys. Rev. B **77**, 085328 (2008).
[197] G. Lommer, F. Malcher, and U. Rössler, Phys. Rev. Lett. **60**, 728 (1988).
[198] J. Nitta, T. Akazaki, H. Takayanagi, and T. Enoki, Phys. Rev. Lett. **78**, 1335 (1997).
[199] J. Li, A. M. Gilbertson, K. L. Litvinenko, L. F. Cohen, and S. K. Clowes, Phys. Rev. B **85**, 045431 (2012).
[200] S. Stachel, P. Olbrich, C. Zoth, U. Hagner, T. Stangl, C. Karl, P. Lutz, V. V. Bel'kov, S. K. Clowes, T. Ashley, A. M. Gilbertson, and S. D. Ganichev, Phys. Rev. B **85**, 045305 (2012).
[201] H. Diehl, V. A. Shalygin, S. N. Danilov, S. A. Tarasenko, V. V. Bel'kov, D. Schuh, W. Wegscheider, W. Prettl, and S. D. Ganichev, J. Phys.: Condens. Matter **19**, 436232 (2007).
[202] H. Diehl, V. A. Shalygin, L. E. Golub, S. A. Tarasenko, S. N. Danilov, V. V. Bel'kov, E. G. Novik, H. Buhmann, L. W. Molenkamp, C. Brüne, E. L. Ivchenko, and S. D. Ganichev, Phys. Rev. B **80**, 075311 (2009).
[203] G. A. Khodaparast, R. E. Doezema, S. J. Chung, K. J. Goldammer, and M. B. Santos, Phys. Rev. B **70**, 155322 (2004).
[204] A. M. Gilbertson, W. R. Branford, M. Fearn, L. Buckle, P. D. Buckle, T. Ashley, and L. F. Cohen, Phys. Rev. B **79**, 235333 (2009).
[205] R. L. Kallaher, J. J. Heremans, N. Goel, S. J. Chung, and M. B. Santos, Phys. Rev B **81**, 075303 (2010).
[206] M. Akabori1, V. A. Guzenko, T. Sato, Th. Schäpers, T. Suzuki, and S. Yamada, Phys. Rev. B **77**, 205320 (2008).
[207] M. A. Leontiadou, K. L. Litvinenko, A. M. Gilbertson, C. R. Pidgeon, W. R. Branford, L. F. Cohen, M. Fearn, T. Ashley, M. T. Emeny, B. N. Murdin, and S. K. Clowes, J. Phys.: Condens. Matter **23**, 035801 (2011).
[208] L. E. Golub, Physica E **17**, 342 (2003).
[209] H. T. Duc, J. Förstner, and T. Meier, Phys. Rev. B **82**, 115316 (2010).
[210] H.-Z. Lu, B. Zhou, F.-C. Zhang, and S.-Q. Shen, Phys. Rev. B **83**, 125320 (2011).
[211] J. L. Yu, Y. H. Chen, C. Y. Jiang, Y. Liu, and H. Ma, J. Appl. Phys. **109**, 053519 (2011).

[212] J. L. Yu, Y. H. Chen, C. Y. Jiang, Y. Liu, H. Ma, and L. P. Zhu, Appl. Phys. Lett. **100**, 142109 (2012).
[213] J. Yu, Y. Chen, S. Cheng, and Y. Lai, Physica E **49**, 92 (2013).
[214] S. A. Tarasenko and N. S. Averkiev, Pis'ma ZhETF **75**, 669 (2002) [JETP Lett. **75**, 552 (2002)].
[215] N. S. Averkiev, M. M. Glazov, and S. A. Tarasenko, Solid State Commun. **133**, 543 (2005).
[216] W. Desrat, D. K. Maude, Z. R. Wasilewski, R. Airey, and G. Hill, Phys. Rev. B **74**, 193317 (2006).
[217] M.-H. Liu, K.-W. Chen, S.-H. Chen, and C.-R. Chang, Phys. Rev. B **74**, 235322 (2006).
[218] J. L. Cheng and M. W. Wu, J. Appl. Phys. **99**, 083704 (2006).
[219] B. A. Bernevig and J. Hu, Phys. Rev. B **78**, 245123 (2008).
[220] J. Li and K. Chang, Phys. Rev. B **82**, 033304 (2010).
[221] V. A. Slipko, I. Savran, Yu. V. Pershin, Phys. Rev. B **83**, 193302 (2011).
[222] V. A. Slipko, A. A. Hayeva, and Yu. V. Pershin, Phys. Rev. B **87**, 035430 (2013).
[223] Note that the electron density and sample temperature can also affect both linear and cubic in $\boldsymbol{k}$ Dresselhaus terms, see Eq. (8), (9) and related discussion. While this influence is small in materials with weak cubic in $\boldsymbol{k}$ spin splitting in narrow band semiconductors like InAs-based QWs it may play an important role, see Section 5.2.
[224] G. Engels, J. Lange, Th. Schäpers, and H. Lüth, Phys. Rev. B **55**, R1958 (1997).
[225] T. Koga, J. Nitta, T. Akazaki, and H. Takayanagi, Phys. Rev. Lett. **89**, 046801 (2002).
[226] S. Faniel, T. Matsuura, S. Mineshige, Y. Sekine, and T. Koga, Phys. Rev. B **83**, 115309 (2011).
[227] M. M. Glazov and L. E. Golub, Semiconductors **40**, 1209 (2006).
[228] T. D. Stanescu and V. Galitski, Phys. Rev. B **75**, 125307 (2007).
[229] M. Duckheim, D. Loss, M. Scheid, K. Richter, I. Adagideli, and P. Jacquod, Phys. Rev. B **81**, 085303 (2010).
[230] M. C. Lüffe, J. Kailasvuori, and T. S. Nunner, Phys. Rev. B **84**, 075326 (2011).
[231] S. Faniel, T. Matsuura, S. Mineshige, Y. Sekine, and T. Koga, Phys. Rev. B **83**, 115309 (2011).
[232] M. Scheid, M. Kohda, Y. Kunihashi, K. Richter, and J. Nitta, Phys. Rev. Lett. **101**, 266401 (2008).
[233] T. Hassenkam, S. Pedersen, K. Baklanov, A. Kristensen, C. B. Sorensen, P. E. Lindelof, F. G. Pikus, and G. E. Pikus, Phys. Rev. B **55**, 9298 (1997).
[234] K. C. Hall, K. Gündoğdu, E. Altunkaya, W. H. Lau, M. E. Flatté, T. F. Boggess, J. J. Zinck, W. B. Barvosa-Carter, and S. L. Skeith, Phys. Rev. B **68**, 115311 (2003).
[235] M. Henini, O. Z. Karimov, G. H. John, R. T. Harley, and R. J. Airey, Physica E **23** 309 (2004).
[236] K. Morita, H. Sanada, S. Matsuzaka, C. Y. Hu, Y. Ohno, and H. Ohno, Appl. Phys. Lett. **87**, 171905 (2005).
[237] K. C. Ku, S. H. Chun, W. H. Wang, W. Fadgen, D. A. Issadore, N. Samarth, R. J. Epstein, and D. D. Awschalom, J. Supercond. **18**, 185 (2005).
[238] J. Hicks, K. Gündoğdu, A. N. Kocbay, K. C. Hall, T. F. Boggess, K. Holabird, A. Hunter, and J. J. Zinck, Physica E **34**, 371 (2006).
[239] O. D. D. Couto, Jr., F. Iikawa, J. Rudolph, R. Hey, and P. V. Santos, Phys. Rev. Lett. **98**, 036603 (2007).
[240] L. Schreiber, D. Duda, B. Beschoten, G. Güntherodt, H.-P. Schönherr, and J. Herfort, Phys. Status Solidi B **244**, 2960 (2007).
[241] L. Schreiber, D. Duda, B. Beschoten, G. Güntherodt, H.-P. Schönherr, and J. Herfort, Phys. Rev. B **75**, 193304 (2007).
[242] S. Eldridge, P. G. Lagoudakis, M. Henini, and R. T. Harley, Phys. Rev. B **81**, 033302 (2010).
[243] S. Iba, S. Koh, and H. Kawaguchi, Appl. Phys. Lett. **97** 202102 (2010).
[244] R. Völkl, M. Griesbeck, S. A. Tarasenko, D. Schuh, W. Wegscheider, C. Schüller, and T. Korn, Phys. Rev. B **83**, 241306(R) (2011).
[245] J. Hübner, S. Kunz, S. Oertel, D. Schuh, M. Pochwała, H. T. Duc, J. Förstner, T. Meier, and M. Oestreich, Phys. Rev. B **84**, 041301(R) (2011).
[246] M. W. Wu and M. Kuwata-Gonokami, Solid State Commun. **121**, 509 (2002).
[247] S. W. Chang and S. L. Chuang, Phys. Rev. B **72** 115429 (2005).
[248] S. A. Tarasenko, Phys. Rev. B **80**, 165317 (2009).
[249] M. M. Glazov, M. A. Semina, and E. Ya. Sherman, Phys. Rev. B **81**, 115332 (2010).
[250] Y. Zhou and M. W. Wu, Europhys. Lett. **89**, 57001 (2010).
[251] A. V. Poshakinskiy and S. A. Tarasenko, Phys. Rev. B **87**, 235301 (2013).
[252] P. Olbrich, J. Allerdings, V. V. Bel'kov, S. A. Tarasenko, D. Schuh, W. Wegscheider, T. Korn, C. Schüller, D. Weiss, and S. D. Ganichev, Phys. Rev. B **79**, 245329 (2009).
[253] H. Zhao, X. Pan, A. L. Smirl, R. D. R. Bhat, A. Najmaie, J. E. Sipe, and H. M. van Driel, Phys. Rev. B **72**, 201302(R) (2005).
[254] V. A. Shalygin, H. Diehl, Ch. Hoffmann, S. N. Danilov, T. Herrle, S. A. Tarasenko, D. Schuh, Ch. Gerl, W. Wegscheider, W. Prettl, and S. D. Ganichev, JETP Lett. **84**, 570 (2006).
[255] H. Diehl, V. A. Shalygin, V. V. Bel'kov, Ch. Hoffmann, S. N. Danilov, T. Herrle, S. A. Tarasenko, D. Schuh, Ch. Gerl, W. Wegscheider, W. Prettl, and S. D. Ganichev, New J. Phys. **9**, 349 (2007) [special issue "Focus on Spintronics in Reduced Dimensions"].
[256] K. G. Hu, Solid State Commun. **148**, 283 (2008).
[257] S. Nakamura, S. Pearton, and G. Fasol, The Blue Laser Diode. The Complete Story (Springer, Berlin, 2007).
[258] Q. Chen, M. Asif Khan, J. W. Yang, C. J. Sun, M. S. Shur, and H. Park, Appl. Phys. Lett. **69**, 794 (1996).
[259] Y.-F. Wu, B. P. Keller, S. Keller, D. Kapolnek, P. Kozodoy, S. P. Denbaars, and U. K. Mishra, Appl. Phys. Lett. **69**, 1438 (1996).
[260] O. Ambacher, J. Smart, J. R. Shealy, N. G. Weimann, K. Chu, M. Murphy, W. J. Schaff, L. F. Eastman, R. Dimitrov, L. Wittmer, M. Stutzmann, W. Rieger, and J. Hilsenbeck, J. Appl. Phys. **85**, 3222 (1999).
[261] T. Dietl, H. Ohno, F. Matsukura, J. Cibert, and D. Ferrand, Science **287**, 1019 (2000).
[262] S. Dhar, O. Brandt, M. Ramsteiner, V. F. Sapega, and K. H. Ploog, Phys. Rev. Lett. **94**, 037205 (2005).
[263] G. M. Dalpian and S.-H. Wei, Phys. Rev. B **72**, 115201 (2005).
[264] S. Dhar, T. Kammermeier, A. Ney, L. Pérez, K. H. Ploog, A. Melnikov, and A. D. Wieck, Appl. Phys. Lett. **89**, 062503 (2006).
[265] M. A. Khaderbad, S. Dhar, L. Pérez, K. H. Ploog, A. Melnikov, and A. D. Wieck, Appl. Phys. Lett. **91**, 072514 (2007).

[266] J. H. Buss, J. Rudolph, S. Shvarkov, F. Semond, D. Reuter, A. D. Wieck, and D. Hägele, Appl. Phys. Lett. **103**, 92401 (2013).
[267] B. Beschoten, E. Johnston-Halperin, D. K. Young, M. Poggio, J. E. Grimaldi, S. Keller, S. P. DenBaars, U. K. Mishra, E. L. Hu, and D. D. Awschalom, Phys. Rev. B **63**, 121202 (2001).
[268] J. H. Buß, J. Rudolph, F. Natali, F. Semond, and D. Hägele, Phys. Rev. B **81**, 155216 (2010).
[269] J. H. Buß, J. Rudolph, S. Starosilec, A. Schaefer, F. Semond, Y. Cordier, A. D. Wieck, and D. Hägele, Phys. Rev. B **84**, 153202 (2011).
[270] W. Weber, S. D. Ganichev, Z. D. Kvon, V. V. Bel'kov, L. E. Golub, S. N. Danilov, D. Weiss, W. Prettl, H.-I. Cho, and J.-H. Lee, Appl. Phys. Lett. **87**, 262106 (2005).
[271] R. Cingolani, A. Botchkarev, H. Tang, H. Morkoc, G. Traetta, G. Coli, M. Lomascolo, A. Di Carlo, F. Della Sala, and P. Lugli, Phys. Rev. B **61**, 2711 (2000).
[272] V. I. Litvinov, Phys. Rev. B **68**, 155314 (2003).
[273] X. W. He, B. Shen, Y. Q. Tang, N. Tang, C. M. Yin, F. J. Xu, Z. J. Yang, G. Y. Zhang, Y. H. Chen, C. G. Tang, and Z. G. Wang, Appl. Phys. Lett. **91**, 071912 (2007).
[274] Y. Q. Tang, B. Shen, X. W. He, K. Han, N. Tang, W. H. Chen, Z. J. Yang, G. Y. Zhang, Y. H. Chen, C. G. Tang, Z. G. Wang, K. S. Cho, and Y. F. Chen, Appl. Phys. Lett. **91**, 071920 (2007).
[275] K. S. Cho, C.-T. Liang, Y. F. Chen, Y. Q. Tang, and B. Shen, Phys. Rev. B **75**, 071912 (2007).
[276] W. Weber, S. Seidl, V. V. Bel'kov, L. E. Golub, E. L. Ivchenko, W. Prettl, Z. D. Kvon, H.-I. Cho, J.-H. Lee, and S. D. Ganichev, Solid State Commun. **145**, 56 (2008).
[277] N. Tang, B. Shen, K. Han, F.-C. Lu, F.-J. Xu, Z.-X. Qin, and G.-Y. Zhang, Appl. Phys. Lett. **93**, 172113 (2008).
[278] K. S. Cho, T.-Y. Huang, H.-S. Wang, M.-G. Lin, T.-M. Chen, C.-T. Liang, Y. F. Chen, and I. Lo, Appl. Phys. Lett. **86**, 222102 (2005).
[279] N. Thillosen, Th. Schäpers, N. Kaluza, H. Hardtdegen, and V. A. Guzenko, Appl. Phys. Lett. **88**, 022111 (2006).
[280] S. Schmult, M. J. Manfra, A. Punnoose, A. M. Sergent, K. W. Baldwin, and R. J. Molnar, Phys. Rev. B **74**, 033302 (2006).
[281] N. Tang, B. Shen, M. J. Wang, K. Han, Z. J. Yang, K. Xu, G. Y. Zhang, T. Lin, B. Zhu, W. Z. Zhou, and J. H. Chu, Appl. Phys. Lett. **88**, 172112 (2006).
[282] D. Spirito, L. Di Gaspare, G. Frucci, F. Evangelisti, A. Di Gaspare, A. Natargiacomo, E. Giovine, S. Roddaro, and F. Beltram, Phys. Rev. B **83**, 155318 (2011).
[283] Z. Zhang, R. Zhang, B. Liu, Z. L. Xie, X. Q. Xiu, P. Han, H. Lu, Y. D. Zheng, Y. H. Chen, C. G. Tang, and Z. G. Wang, Solid State Commun. **145**, 159 (2008).
[284] Q. Zhang, X. Q. Wang, X. W. He, C. M. Yin, F. J. Xu, B. Shen, Y. H. Chen, Z. G. Wang, Y. Ishitani, and A. Yoshikawa, Appl. Phys. Lett. **95**, 031902 (2009).
[285] Z. Zhang, R. Zhang, Z. L. Xie, B. Liu, M. Li, D. Y. Fu, H. N. Fang, X. Q. Xiu, H. Lu, Y. D. Zheng, Y. H. Chen, C. G. Tang, and Z. G. Wang, Solid State Commun. **149**, 1004 (2009).
[286] J. X. Duan, N. Tang, J. D. Ye, F. H. Mei, K. L. Teo, Y. H. Chen, W. K. Ge, and B. Shen, Appl. Phys. Lett. **102**, 192405 (2013).
[287] H. Malissa, W. Jantsch, M. Mühlberger, F. Schäffler, Z. Wilamowski, M. Draxler, and P. Bauer, Appl. Phys. Lett. **85**, 1739 (2004).
[288] A. M. Tyryshkin, S. A. Lyon, W. Jantsch, and F. Schäffler, Phys. Rev. Lett. **94**, 126802 (2005).
[289] J. Matsunami, M. Ooya, and T. Okamoto, Phys. Rev. Lett. **97**, 066602 (2006).
[290] S. D. Ganichev, S. N. Danilov, V. V. Bel'kov, S. Giglberger, S. A. Tarasenko, E. L. Ivchenko, D. Weiss, W. Jantsch, F. Schäffler, D. Gruber, and W. Prettl, Phys. Rev. B **75**, 155317 (2007)
[291] C. M. Wei, K. S. Cho, Y. F. Chen, Y. H. Peng, C. W. Chiu, and C. H. Kuan, Appl. Phys. Lett. **91**, 252102 (2007).
[292] S. D. Ganichev, J. Kiermaier, W. Weber, S. N. Danilov, D. Schuh, Ch. Gerl, W. Wegscheider, D. Bougeard, G. Abstreiter, and W. Prettl, Appl. Phys. Lett. **91**, 091101 (2007).
[293] S. D. Ganichev, E. L. Ivchenko, H. Ketterl, W. Prettl, and L. E. Vorobjev, Appl. Phys. Lett. **77**, 3146 (2000).
[294] D. A. Vasyukov, A. S. Plaut, and M. Henini, Physica E **42**, 964 (2010).
[295] D. A. Vasyukov, A. S. Plaut, A. H. Macdonald, and M. Henini, Int. J. Mod. Phys. B **23**, 2867 (2009).
[296] A. Lorke, S. Wimmer, B. Jager, J. P. Kotthaus, W. Wegscheider, and M. Bichler, Physica (Amsterdam) **249–251B**, 312 (1998).
[297] P. Olbrich, J. Karch, E. L. Ivchenko, J. Kamann, B. März, M. Fehrenbacher, D. Weiss, and S. D. Ganichev, Phys. Rev. B **83**, 165320 (2011).
[298] P. Olbrich, E. L. Ivchenko, T. Feil, R. Ravash, S. D. Danilov, J. Allerdings, D. Weiss, and S. D. Ganichev, Phys. Rev. Lett. **103**, 090603 (2009).
[299] E. S. Kannan, I. Bisotto, J.-C. Portal, R. Murali, and T. J. Beck, Appl. Phys. Lett. **98**, 193505 (2011).
[300] E. L. Ivchenko and S. D. Ganichev, JETP Lett. **93**, 673 (2011).
[301] Ch. Jiang, Y. Chen, H. Ma, J. Yu, and Y. Liu, Appl. Phys. Lett. **98**, 232116 (2011).
[302] S. D. Ganichev, S. A. Tarasenko, V. V. Bel'kov, P. Olbrich, W. Eder, D. R. Yakovlev, V. Kolkovsky, W. Zaleszczyk, G. Karczewski, T. Wojtowicz, and D. Weiss, Phys. Rev. Lett. **102**, 156602 (2009).
[303] Ya. V. Terent'ev, C. Zoth, V. V. Bel'kov, P. Olbrich, C. Drexler, V. Lechner, P. Lutz, A. N. Semenov, V. A. Solov'ev, I. V. Sedova, G. V. Klimko, T. A. Komissarova, S. V. Ivanov, and S. D. Ganichev, Appl. Phys. Lett. **99**, 072111 (2011).
[304] P. Olbrich, C. Zoth, P. Lutz, C. Drexler, V. V. Bel'kov, Ya. V. Terent'ev, S. A. Tarasenko, A. N. Semenov, S. V. Ivanov, D. R. Yakovlev, T. Wojtowicz, U. Wurstbauer, D. Schuh, and S. D. Ganichev, Phys. Rev. B **85**, 085310 (2012).